POLITECNICO DI TORINO

Facoltà di INGEGNERIA

Corso di Laurea Magistrale in Ingegneria Aerospaziale

Tesi di Laurea Magistrale

Development of biodegradable mini-radiosondes to measure fluctuations in pressure, temperature, humidity, velocity within warm clouds

Thesis associated with the EU project H2020

MSCA ITN ETN COMPLETE

Relatore

prof.ssa Daniela Tordella

Giovanni Cipri

Dicembre 2020

Abstract

The microphysical processes that take place within warm clouds are a source of uncertainty for current meteorology: several gaps exist in the knowledge of the growth of droplets in the clouds and the subsequent development of rain. One of the factors that makes it very uncertain is the role that turbulence plays in the microphysical processes that involve the growth of droplets: CCN (Cloud Condensation Nuclei), condensation, collision. The great knowledge lacks that there are on the subject are probably due to the limited amount of data taken in the field, with sensors transmitting data from the clouds. Even less has been, until now, the data captured by a probe capable of faithfully following the trajectories of the current in the clouds, that is in a Lagrangian way. The COMPLETE project, a Horizon2020 programme, was created to broaden the knowledge science has about the interaction between turbulence (from small to large scales) and microphysical phenomena in the clouds, thanks to the use of a floating, disposable, biodegradable, radio probe capable of transmitting data in real time to a ground receiver on pressure, temperature, humidity, trajectory and speed. In particular, in this thesis, after having discussed and illustrated the current gaps in knowledge on the subject, it is intended to report: the main components of the radiosonde; the operating principle; the assembly procedures optimised by the author in the IIT laboratories; the first data captured by the probe.

Contents

Chapter 1

Introduction

Humans have observed and investigated clouds and weather phenomena for thousands of years, trying to understand and eventually predict their behaviour. It has always been, therefore, of crucial importance for life on our planet the knowledge of clouds, in order to better organize agriculture, to foresee disasters or droughts. However, despite the technological evolution of the instruments that enable atmospheric observations (satellites, probes, computational calculations), even today the gaps concerning several physical and chemical phenomena which take place inside the clouds are mostly unknown, or at least not confirmed. Indeed, clouds involve large scale motions that are connected through complicated and sometimes unexplained processes to micro-physical and micro-chemical phenomena.

One of the reasons for such gaps in the knowledge of cloud evolution is the scarcity of in-situ measurements along Lagrangian trajectories, which could provide very important information about the fluctuations of many physical and chemical quantities, from large to small scales [1]. Precisely to meet the necessity for this type of measurement, a small radiosonde was developed as part of the Horizon2020 Innovative Training Network Cloud-MicroPhysics-Turbulence-Telemetry (MSCA-ITN-COMPLETE) project [2], capable of floating in the clouds and following Lagrangian trajectories. Moreover, the probe is designed to be disposable, so it has to be biodegradable, cheap and simple to produce.

The radiosonde must thus satisfy the above mentioned characteristics in order to meet the project objectives. Firstly it must succeed in transmitting data regarding the point where it is located (pressure, temperature, humidity, position, speed) in real time, to a

ground receiver: it must therefore contain different types of sensors, a battery and micro-electronic components capable of processing and sending the data. A further important objective is to follow the trajectories of the current in a Lagrangian way, so the probe must float at a certain height and must have reduced dimensions so as to achieve reduced inertia: the various sensors are inserted inside a balloon filled with helium, with a diameter not exceeding 40cm. To ensure that the probe is both small and fluctuates, the materials used must remain as light as possible. Finally, as already mentioned, the probe will most likely be dispersed in the environment and not reusable, so it must be inexpensive, easy to produce several units, biodegradable.

During the time I was involved in the COMPLETE project, I had the objective to work on the structure of the mini radio-probe. I analysed the right dimensions and weights so that the probe could fluctuate at the right altitude; I studied the right shapes of the balloon so that it would faithfully follow the Lagrangian fluctuations of the current; I designed and realized a structure so that the board containing the sensors would lie in the centre of the balloon, without adding weight to it. This phase of the work was carried out at the Smart Materials department of the IIT (Italian Institute of Technology), which collaborates on the project having previously analysed and chosen the material used for the balloon [3]. I subsequently collaborated in the realization of some tests carried out to examine the probe as a whole, analyzing the data received from it.

In the following chapter of the thesis, which is purely bibliographic, an overview of current knowledge on the role of turbulence in the development of clouds and atmospheric precipitation is presented: growth by condensation and collision of cloud droplets in a large and small scale turbulence, entrainment and detrainment in a turbulent environment. Within the third chapter, an account is given of the current development of the various components of the radiosonde, an operating principle is outlined and the data characterising the instrument in question is provided. Chapter 4 presents the production protocol of the balloon developed by me in IIT: it shows the calculations realized, the tools used, the methodologies to be applied for the radiosonde to meet the requirements. Chapter 5 shows the results obtained from the real preliminary tests carried out in the field: data concerning position, speed, pressure, temperature, relative humidity; data concerning some tests on the material chosen for the balloon.

The results obtained from the preliminary tests highlight some determinants for which the radiosonde needs to be perfected but, nevertheless, confirm that the probe is able to collect information and transmit it, following the Lagrangian fluctuations of the current at altitudes of 1000m for over an hour.

Chapter 2

Clouds as source of uncertainty

2.1 Cloud formation

A parcel of atmospheric air is characterized by a *mixing ratio*, that is the content of water vapor (measured in g) per kilogram of dry air; this quantitative can be expressed also not dimensionally as *relative humidity* [4]. There is a limit of mixing ratio value for which air becomes saturated and it is not able to contain more water vapor (here it is said that *relative humidity* is 100%). *Supersaturation* is defined as the relative degree of water-vapor pressure exceeding the saturation vapor pressure. From the moment that the air is super-saturated, formation of cloud takes place [5].

The value of water vapor to which air becomes saturated depends on the atmospheric temperature. The temperature to which air must be cooled in order to become saturated is called *dew point*. Cooler air can contain less water vapor than warmer air before becoming saturated, so its dew point is lower. A parcel of air typically tends to rise due to convection, large scale atmospheric motions, or orographic lift(presence i.e. mountains). Rising, air expands and cools, up to the dew point, where clouds are formed. [6]. The mechanism above described is called *adiabatic cooling*, which is the more frequent. Nevertheless, other types of cooling exist: conductive, radiational, evaporative, which are of relatively limited interest in the analyses carried out in this work.

8

2.1.1   Cloud forms and levels

Several types of clouds classification exist in bibliography: there are different types: from the simple ones to study to those for which uncertainties are still many, due to the strong instability to which they are subjected. A simplified classification of cloud types is below reported:

- *Stratiform* clouds (Figure 2.1) are the most stable type. This kind of cloud presents generally flat, sheet-like structures and it rarely produce precipitation. This type of cloud can be found at every level of the troposphere and does not produce precipitations [7].

Figure 2.1: Wavy stratiform clouds over Sterling, Virginia (USA) [7]

- *Cirriform* clouds are in filament forms (Figure 2.2) and they are mostly stable.This kind of cloud is present only in high tropospheric altitudes and does not produce precipitations [7].

- *Stratocumiliform* clouds (Figure 2.3) have both stratiform and cumuliform characteristics. These clouds are mostly stable and precipitations depend on altitude at which the cloud is located [7].

- *Cumuliform* clouds (Figure 2.4) have instability which grow with their dimensions. This type of cloud has heaps or tufts shapes, and might be low-level or multi-level(in this case precipitations remains abundant) [7].

9

Figure 2.2: Picture taken of a cirriform cloud [7]
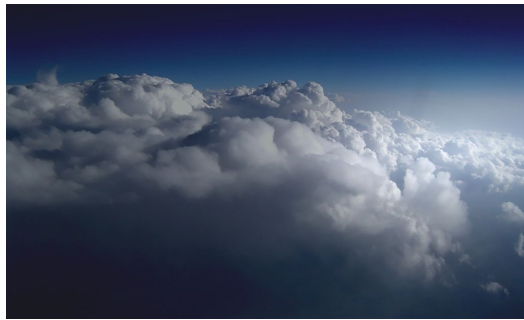
Figure 2.3: Picture taken of a stratocumulus cloud [7]

Figure 2.4: Picture taken of a cumulus cloud [7]

- *Cumulonimbiform* clouds (Figure 2.5) have towering vertical extent. They present high turbulence and instability and can produce moderate to heavy showers [7].

2.2 Activation and growth of droplets in warm clouds

Warm clouds droplets activation and growth up to raindrop size take place through three fundamental steps:

1. CCN activation;

Figure 2.5: Picture taken of a cumulonimbus cloud [7]

2. Growth for diffusion/condensation of water vapour;

3. Growth for collision/coalescence

The large and small scale physical and chemical mechanisms involved in the three phases of warm clouds formation are explained below.

2.2.1   CCN activation

CCNs (Cloud Condensation Nuclei) are atmospheric aerosols of some micron, originated by micro-particles deeply higroscopics (i.e. dust or chloride) on which water vapor tends to condensate [8], [9].

It is possible to notice that the number of CCN increases with increasing supersaturation. First to be activated to form drops are largest and most effective CCN, followed by smaller ones, until supersaturation level stop rising and starts to decrease, just above the cloud base. At this stage the process of activation of the CCNs can be defined as completed, droplet concentration has been determined and growth for diffusion can start. The radius of a micro-droplet, at the end of CCNs activation process, results $\sim 1\mu m$ [9], [10].

Studies and laboratory tests [11] demonstrated that also falling hail and cool rain drops may cause or facilitate the nucleation process of cloud droplets. Inside wakes generated

11

by the fall, under supersaturated atmospheric conditions,nucleation of micro-droplets may result enhanced.

2.2.2   Growth for diffusion and condensation of water vapour

Droplet growth rate for condensation is inversely proportional to its radius (r), and determined largely by supersaturation level (s). In fact this rate can be represented by the following equation [12]:

$$\frac{dr}{dt} \propto \frac{s}{r} \tag{2.1}$$

Because small-sized droplets growth is faster than droplets with bigger radii, it is possible to argue that droplet size distribution at this stage of the droplet growth (an example is shown in Figure 2.6) is narrower as mean droplet radius increases, provided all particles are exposed to the same supersaturation - the big ones starts to grow slowly and the small ones achieve them [10], [8], [9].

It must be said, however, that, in normality, droplets are not all exposed to the same level of supersaturation (or more precisely the same value of integral s along the trajectory). Indeed, in real clouds droplets do not evolve in adiabatically closed cells, but they come into contact with other more or less evolved particles (because turbulence and/or entrainment) or they are exposed to inhomogeneities in the field of supersaturation [13]. The outcome is that the resulting spectrum after the condensation phase is not as narrow as the analytical formulas would suggest (as shown in Figure 2.6), but tends, thanks to the phenomena described above, to widen and, thanks to this widening, to favor the future process of coalescence

Growth for diffusion and condensations occurs efficiently for droplets with radii smaller than $15 - 20\mu m$ [10], beyond which it becomes negligible. Diffusional growth is a reversible process, as opposed to growth by collision-coalescence, which is defined as irreversible process [14].

2.2.3   Growth for collision and coalescence

During this phase, larger droplets capture smaller ones by gravitational attraction and in this way mean size of droplets continues to grow [8]. Increasing particles size, and
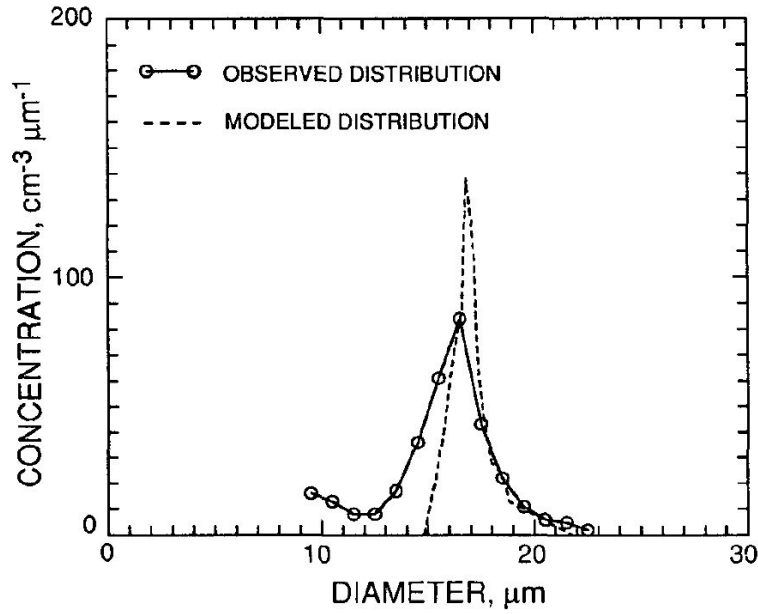
Figure 2.6: Typical observed and modeled distribution during diffusional range [9]

consequently their terminal velocity and their inertia, the growth rate by coalescence is enhanced. This occurs because small droplets tends to follow streamlines of the air flowing around large ones, while larger droplets are hindered to do it because of their inertia, so they coalesce [12], [14]. For this reason, the larger the difference between droplets, the greater the collision rate results. In terms of droplets size distributions, this phenomenon means that the frequency of droplet collisions depends on the droplet spectrum width. It follows that understanding processes leading to the observed droplet spectra is important for the understanding of the rain onset [15].

Another important determinant of the collision rate between particles within the cloud is altitude. Altitude is a factor that can increase the terminal velocity of the droplet (from 5% to 20%) and consequently enhance the collision efficiency: lower air pressure and density values would make the motion of the particles much freer, guaranteeing a higher speed [16].

One of the most significant gaps in the knowledge of the growth processes of droplets in the clouds is the fact that the collision/coalescence process take place for droplets bigger than $\sim 40\mu m$. This fact creates a *bottleneck size range*, because it is poorly understood how droplets grow from the end of diffusional range ($\sim 20\mu m$) to the beginnings of collisional range [17].

13

2.3 Cloud structure

Water concentration within a typical cloud (cumulus, stratocumulus) spans from $10 - 100 droplets/cm^3$ for small-sized droplets to $1 droplet/cm^3$ for droplets with radii $> 250 \mu m$. In other words, as mean radius increases, water concentration decreases, consequently spectrum peaks move to the right and downwards, broadening the spectrum shape. At the same way, the higher is water concentration, narrower is spectrum and mean size is typically small [8].

It is necessary now to focus on the shape of the droplets spectrum as a function of the location within the cloud. Firstly, a cumulus cloud will be crossed vertically, then it will be observed how the concentration of the droplets varies through the horizontal extension of the cloud.

- Vertical variability in the cloud: as shown in in Figure 2.7, aircraft measurements [18] in cumulus clouds led us to observe that changes in concentration and size are not significant going up through the cloud.
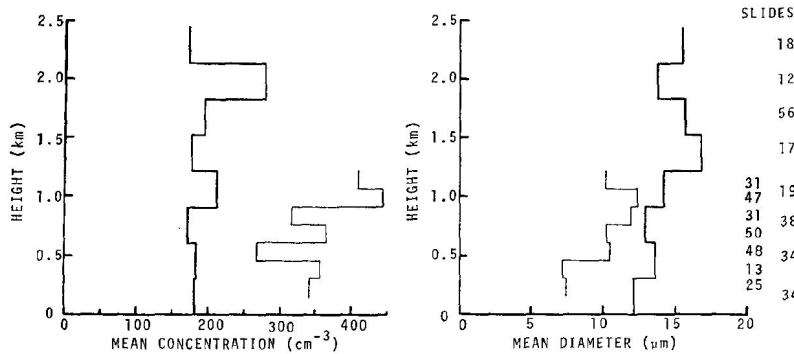

Figure 2.7: The variation with height of droplet concentration and mean diameter averaged in cumulus clouds, from the base to the top of the cloud [18]

However, it is present an increase in the range of large droplets that have low concentrations. Consequently, as shown in Figure 2.8, is visible a slight widening of the spectrum as the measurements were taken towards the cloud top, as well as an increase in frequency of bimodal distribution.
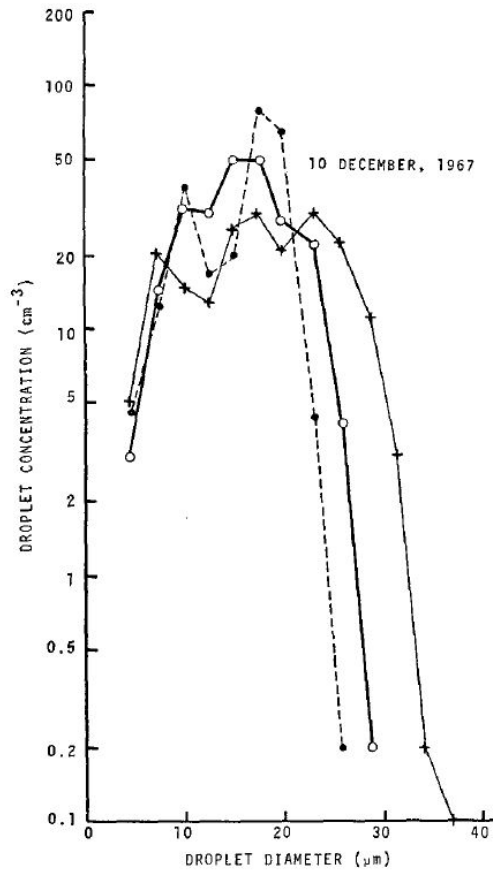
14

Figure 2.8: Three average spectra for different heights above the cloud base. $\bullet$: $600m$; $\circ$: $1100m$; $+$: $1800m$ [18]

- Horizontal variability: it is possible to observe broad regions of homogeneous droplets distribution (*a* in Figure 2.9), interrupted by micro-zones of some centimeters where droplet concentration is near to zero (*b*). Furthermore, very sharp interfaces can be seen between cloud and still air (*c* and *d*) [12]. However, even in the case of region of liquid water content fairly constant throughout the length of the cloud, the spectra noticed in Figure 2.10 are bimodal, and not only at the edges

2.4 Effects of turbulence on cloud dynamics

Clouds are deeply non-stationary, inhomogeneous, intermittent. Inside them, there are strong couplings across different spatial and temporal turbulent scales. So, both fluid dynamics and microphysical processes play an important role in cloud evolution, because
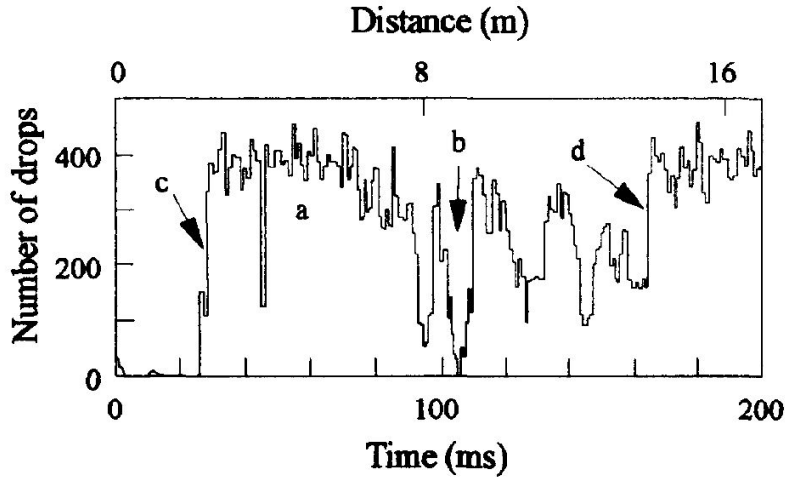
15

Figure 2.9: Droplet concentration measured at 1000 Hz during a flight through a small cumulus cloud, from [19]
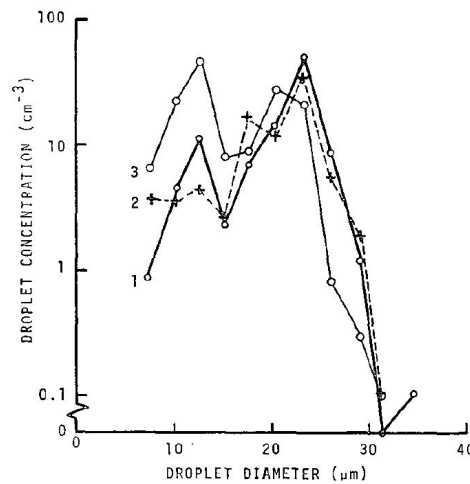
Figure 2.10: Spectra obtained thanks to aircraft measurements [18] flying at 300m above the cloud base

they affects droplets growth and evaporation and, consequently, precipitations and clouds radiative properties [20].

Furthermore, it should also be borne in mind that turbulence play an important role almost exclusively on *warm clouds*, which are clouds without ice-particle contents. In facts, growth by sublimation in much more rapid than growth for condensation, not allowing to turbulence the possibility to enhance cloud particle growth or to modify observed droplet spectra [12].

16

2.4.1 Reference quantities for turbulence in clouds

In the atmospheric boundary layer, and in cumulus clouds, the biggest scale (*integral scale*) is typically of the order of 100m, up to arrive, through the inertial cascade, to the smaller scale (*dissipation scale*), which is typically around 1mm [21]. In the field of studying turbulence within clouds, the term "large scale" corresponds to the range of the local peak in the energy spectrum and is related to the scale at which the kinetic energy is supplied into the turbulent motion; "small scale" or "dissipation scale" refers to the range at which the viscous dissipation converts directly the kinetic energy into heat. Large-scale eddies are often meant [14] to be energy-contained eddies strongly affected by forcing of the flow and by boundary conditions. In contrast, small-scale eddies are assumed to have universal properties, independent of the forcing and boundary conditions.

Besides, observations ([12], [22]) show that typical *turbulent energy dissipation rates* (ϵ) are around $10^{-4}\frac{m^2}{s^3}$ in stratocumulus clouds, $10^{-3}\frac{m^2}{s^3}$ in small cumulus clouds, and a mostly variable range of 10^{-4} to $10^{-1}\frac{m^2}{s^3}$ in precipitating clouds. Estimated Taylor Reynolds numbers (Re_λ) are in the order of 10^4 (but higher in cumulus than stratocumulus clouds), which indicates the turbulence is fully developed. However, it should be kept in mind that turbulent energy dissipation rate is a very uncertain variable across the cloud: below the cloud base it is thought [22] to have a much smaller value than inside, but at the same time, DNS [23] showed that ϵ reach a maximum near the cloud top, probably because of entrainment and mixing with clear air.

2.4.2 Turbolence as a source of uncertanty

Despite the above mentioned data, turbulence in clouds remain a source of uncertainty, in spite of technological development of both computers for simulations and laboratory and in-situ facilities for experiments. Particularly, it is not always easy to establish how and in what quantity turbulence influences micro-physical processes into the clouds because of this following reasons [21]:

- large range of spatial scales of turbulence;

- large Reynolds numbers in atmosphere boundary layer, for which simulation results very high-requiring for computers and difficult to reproduce in wind tunnels;

- multi-phase nature of clouds, which make difficult reconstructing dynamics from instantaneous statistical measurements;

- rare events in the systems, which places several burdens on measurement requirements.

One of the most challenging goals for turbulence study is obtaining adequate estimates of statistical moments through averaging, because boundary condition, in clouds, are frequently not well defined [21].

2.4.3 As turbulence influences the development phases of cloud droplets

Notwithstanding the several uncertainties, what decades of studies, numerical simulations, laboratory tests and in-situ experiments have come to agree is that turbulence, both small and large scale, plays a key role in the growth of droplets and the formation of rain. A study [24], for example, has shown that under conditions similar to those in cumulus clouds, turbulence shortens the formation time of drizzle drops by up to 40% compared to the case of absence of turbulence; other studies (such as [25]) show that as ϵ reaches the value of $1000\frac{cm^2}{s^3}$, the conversion rate of cloud droplets in raindrops can improve by about 50%. Basically, the reasons why turbulence facilitates the growth of droplets and the formation of rain can be summarized in the following 4 points:

- promotion of droplet clustering [26], enhancing coalescence and consequently the growth rate (Figure 2.11);

- yielding entrainment and consequently reducing the cloud water content [12];

- leading to supersaturation fluctuations as shown in Figure 2.12 so that condensation growth can be improved [27];

- influence on the micro-physical development giving rise to broadening of the droplet spectrum, hence increasing the growth rate for coalescence (after condensation had tightened it) [12];

A further effect of the turbulence is to accelerate even more the droplets that are falling under the effect of gravity. This happens because, due to sedimentation (inertia), the
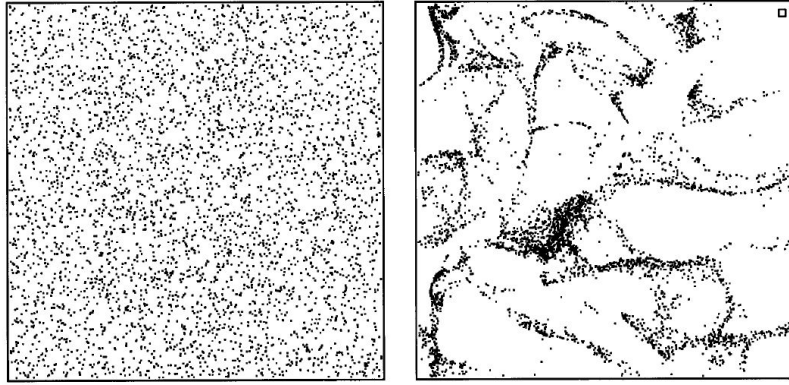
Figure 2.11: Initial (random) particle locations on the left and particle locations after several eddy turnover times (on the right) carried out in a DNS study [26]
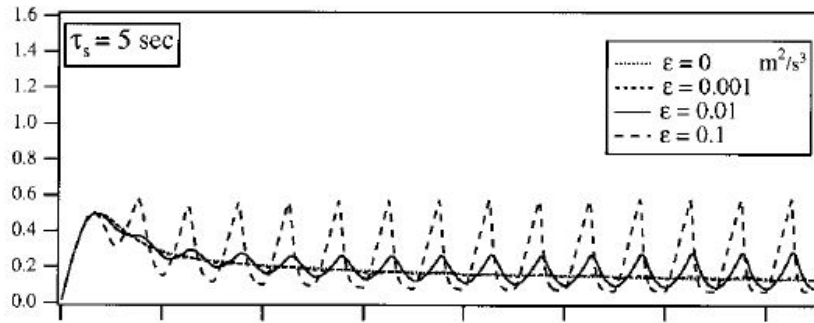

Figure 2.12: In this figure it is possible to notice how the fluctuations in the supersaturation level increase as the turbulence intensifies (ϵ) [26]

droplets deviate towards the downward side of the vortex tube that pushes down, thus accelerating the fall even more [14].

Turbulence effects on diffusional growth

Calculations [12] led to hypothesis that increasing the time during which only few droplets are exposed to supersaturation, growth of large droplets is facilitated. This occurs because droplets grown in more active region (low concentration, high supersaturation) are obviously larger than droplets grown in other regions. After some times, these active region starts to decay, the growth of larger droplets slows down and the spectrum tends to narrow, as expected. Large scale turbulent motion might move a portion of these larger droplets towards region that are beginning now to be more active, allowing them to undergo further condensational growth, broadening spectra (see Figure 2.14) and consequently enhancing future coalescence.
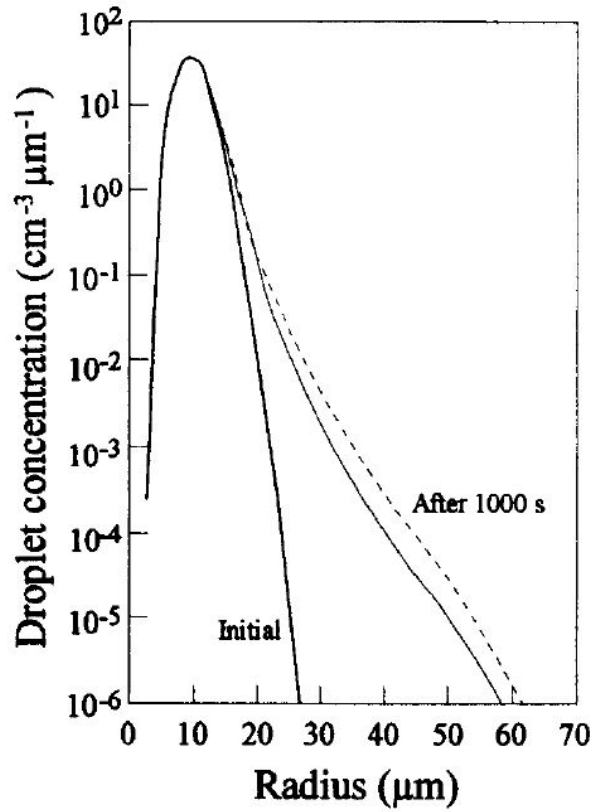
19

Figure 2.13: Calculated spectrum widening [12] if the supersaturation time has increased

However, also small-scale motions can play an important, although sometimes ambiguous, role in droplets growth process. In fact , [26] showed that concentration fluctuations induced by small-scale turbulence lead to fluctuations in supersaturation field. The result is an enhanced growth of large individual droplets and consequently a widening of the spectrum, facilitating the future collision process. Nevertheless, [28] applied a microscopic approach to the growth of cloud droplets and observed that one of the effects of small-scale turbulence (considered alone) is to shorten the characteristic timing of concentration and supersaturation inhomogeneities. In practice, if the *rate of dissipation of turbulent kinetic energy*(ϵ) rises, it results an increase in the instantaneous standard deviation of supersaturation fluctuations (as already shown in Figure 2.12), thus droplets are exposed for less time to supersaturation peaks and large droplets do not grow significantly as described by [26], reducing the spectral widening.

Turbulence effects on cloud droplets collision

Turbulence produces random large-scale accelerations that, added to droplets inertia, create complex trajectories of particles in clouds. This process leads to droplet *clustering* and, hence *collision rate* increase, reducing the time required to form precipitation in clouds [20]. In other words, air turbulence can accelerate droplet collisional growth by increasing the relative velocity and enhancing coagulation effects. Consequently, turbulence can accelerate the onset of warm rain in shallow convective clouds as well as increase its intensity [29]. It is therefore evident that clustering plays a fundamental role in the growth of droplets and consequently in the formation of rain at this stage of evolution. Clustering enhances if the difference in size between droplets increases [14], this is because droplets of different inertia respond differently to changes in flow, and this is another reason why the spectrum needs to be wide in the coalescence phase. In addition, DNSs studies [30] have noted how the effect of gravity facilitates clustering of large droplets.

Large eddies are mainly responsible for droplets generation and growth but also small-scale turbulence play a key role on droplet development. In fact, smaller eddies are needed to allow particles to move from a large eddy to another. This process is known as *large eddy hopping* [10]. Thanks to this moving across large eddies, droplets of different sizes coexist in a small volume and, consequently, collisional growth rate is enhanced [14].

2.4.4 Droplet motion

To study and understand preferential concentration and motion of cloud droplets, two non-dimensional number [28] are important:

- Stokes number:

$$St = \frac{\tau_d}{\tau_\eta} \tag{2.2}$$

where τ_d is the *particle response time*, which is defined as the characteristic time a particle takes to react to changes in flow, while τ_η is the *Kolmogorov timescale*. Since $\tau_\eta = (\nu/\epsilon)^{1/2}$, where ν is the kinematic viscosity of the air, it follows that $St \propto (\epsilon)^{1/2}$.

21

If $St \gg 1$, particles react very slowly to flow changes, while with $St \ll 1$ they follow the flow exactly. It is expected that preferential concentration results when $St \approx 1$ [28].

Stokes number is also important to understand the relative speed between the particles, with consequences on their possibility of collision. In fact, if we consider a monodisperse fluid (all droplets equally sized),

- the relative velocity between the droplets and the flow will be very low for $St \ll 1$ because all the particles will follow the flow very well;

- for $St \simeq 1$, there will be a maximum relative velocity;

- The value will go back down for $St \gg 1$ because of the inertia of the droplets.

For a bidisperse fluid, the trend will be very similar, but with much higher relative velocity values, because particles of different sizes have different inertia and will follow the flow in a different way [31]. Furthermore, if one considers gravity effects, it will get a clear amplification of relative velocity values [30]. Relative speed of droplets and particle clustering are closely linked, and for this reason the clustering values are maximum at St numbers about 1. To confirm what just said there are results from numerous laboratory experiments both of box turbulence (e.g. [32]) and wind tunnel experiments(e.g. [33]) that, in addition to confirming the Stokes value for which the coalescence has enhanced, also reveal that clustering is facilitated for turbulence scales around 10η

- Non-dimensional terminal velocity:

$$Sv = \frac{V_T}{\nu_\eta} \qquad (2.3)$$

where V_T is the *particle terminal velocity*, while ν_η is the *Kolmogorov velocity scale*. Sv significance is the importance of sedimentation in reducing the time of interaction between a droplet and an eddy whose size is equals the *Kolmogorov lenght scale*: if $Sv \gg 1$, particles react very slowly with eddies, while with $Sv \ll 1$, the sedimentation can be neglected.
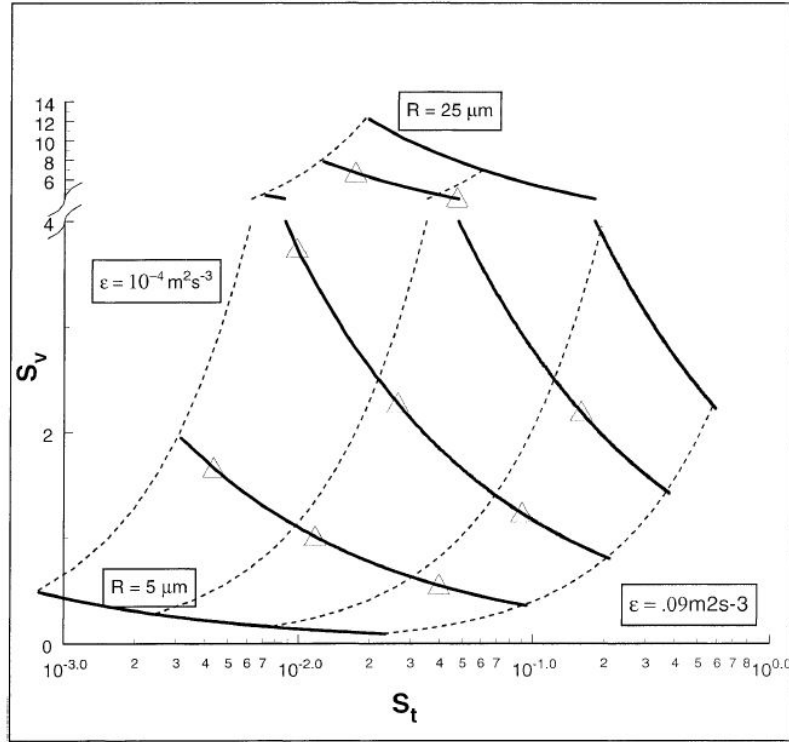
Figure 2.14: Tipical trend between St and Sv varying the turbulence level (ϵ, dashed line) and radius(R) [28]

In [34] it was obtained an analytical equation which represent the motion of a small droplet in a turbulent flow field. Making several simplifications, the equation results:

$$\frac{dv_i}{dt} = g_i + \frac{u_i - v_i}{\tau_d} \tag{2.4}$$

where v_i is the droplet velocity ($_i$ is the direction), u_i represent the flow velocity, g_i the gravity acceleration and τ_d is *inertial droplet response time*. In the limit of Stokes number $St \ll 1$ (where $St = \tau_d/\tau_\eta$, with τ_η is Kolmogorov timescale), (2.4) becomes:

$$v_i \simeq u_i + \tau_d g_i - \tau_d a_l \tag{2.5}$$

The a_l term represent Lagrangian acceleration of the fluid at the particle location. Looking at equation (2.5), it can be understood that droplets tend to move with surrounding air (u_i), but with a **relative motion** resulting by:

- gravitational settling

- inertial response of droplets to flow accelerations

23

2.5   Entrainment in clouds

Entrainment is defined as the mixing of environmental,subsaturated air inside a cloud so that the first one becomes part of the second one. Detrainment is the opposite process:Supersaturated air is forced out of the cloud by certain movements, and once outside the cloud, the droplets present evaporate. Studying these phenomena is crucial to resolve several climate models [35].

2.5.1   Mechanism for entrainment

The process of entrainment of dry air insidethe cloud basically takes place through 3 main steps [14]:

1. *Engulfment* or *nibbling* of dry air inside the cloud through the action of turbulence;

2. Formation of mostly separate clean air and cloudy air filaments, phenomenon known as *stirring* [36];

3. The filaments gradually become increasingly smaller, until they reach sizes in the order of η, a measure to which they become homogenized.

The term *engulfment* is often used to describe the phenomenon when it occurs due to large scale turbulent motions, while *nibbling* is used for small scale. Simulations and laboratory experiments [37] have shown that nibbling is a more often dominant process than engulfment, whereby it appears that molecular diffusion could be the dominant process. This is true if the level of instability resulting from turbulence does not increase significantly, because then *nibbling* would seem to become negligible [37]. The way in which entrainment occurs within a cloud, whether by *engulfment* or *nibbling*, could have important implications for the nature of the mixing process and the measure of spectrum widening that entrainment normally generates [14], [38] (see Figure 2.15) .

In addition to the already cited turbulent entrainment, an irreversible process by which a fluid particle approaches to the turbulent zone and acquires vorticity becoming part of it [36]; also a cloud entrainment exists, a process by which a fluid particle acquires liquid water approaching to cloud and become part of it (de Roode Wang 2007).
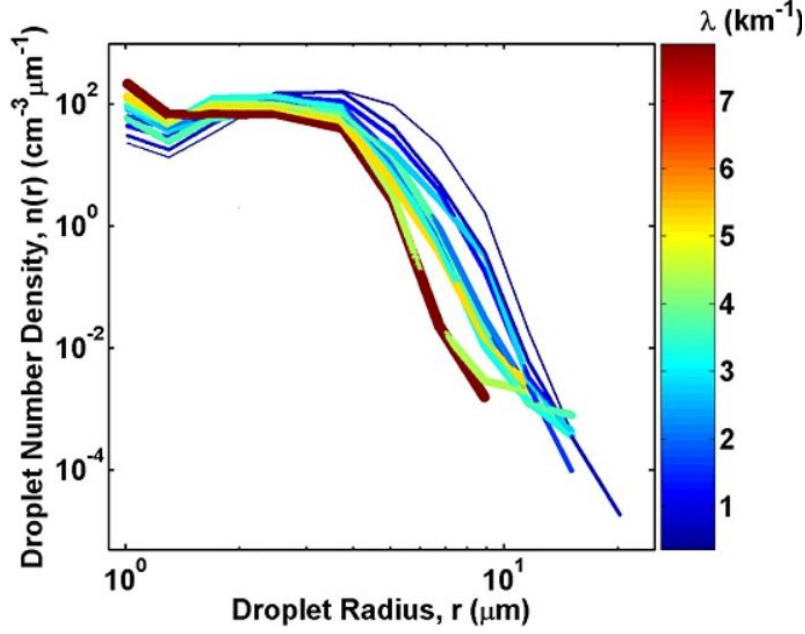
Figure 2.15: Enlargement of the observable spectrum as the rate of entrainment increases (λ) [38]

2.5.2 Consequences of entrainment

One of the main global effects caused by entrainment is the reduction of the liquid water content inside the cloud, with significant consequences on the evolution of cloud droplets and the formation of rain. Entrainment plays a significant role in cumulus clouds rather than stratocumulus, in fact in the former most droplets exhibit evaporation, reducing in size and decreasing the global liquid water content within the cloud, while in the latter this phenomenon happens at about the same speed as the dilution of the droplet number concentration [18], [39].

Entrainment can cause *CCN activation* above the cloud base: clear air supersatured interacts with swirling structures associated with instability at the interface between the cloud and the environment [40]. As a result, it penetrates inside the cloud, raising the level of supersaturation and thus promoting the activation of CCN. —Mixing lead to bimodal spectra [18]

If we consider a parcel with a certain supersaturation level which is subjected to mixing with a lower supersaturation level, it can be noticed that broadening of the spectrum occurs. This type of mixing, in fact, slows the *condensational growth* of larger drops because the average supersaturation is lowered. Besides, larger droplets grow more rapidly

if updrafts containing few droplets occurs and evaporate slowing in downdrafts containing many droplets [9].

We now introduce the *Damköhler number*:

$$Da = \frac{\tau_r}{\tau_s} \tag{2.6}$$

, where τ_r is the characteristic time of a turbulent vortex of radius r, while τ_s is the characteristic time of a thermodynamic reaction related to the case under examination [14].

- If $Da \gg 1$, turbulent fluctuations are slow compared to thermodynamic reactions and can be in some cases neglected. As for the entrainment, in this case we speak of *inhomogeneous entrainment*, because the typical evaporation caused by the phenomenon cannot act uniformly, so some droplets will evaporate while others will remain unchanged. In other words, droplets mixed with dry air will evaporate before being mixed in the cloud. Hence, filaments of air without droplets (which have evaporated) will remain inside the cloud until the air becomes over-saturated. The effect of this type of mixing is a decrease in the number of droplets, while the average size will remain unchanged, so the shape of the spectrum does not change. The fact that the concentration is lower leads to an increasing supersaturation and therefore could also enhance growth of the larger droplets [12].

- When $Da \ll 1$, the opposite happens. In this case the evaporation rate is the same for all the droplets, so they will all evaporate, but slightly, so that the number of droplets does not decrease, but the average diameter of all of them decreases. In this case of homogeneous mixing, then we consider the instantaneous entrainment, so fast that it does not consider the horizontal variability that could be caused by evaporation the spectrum widens because the supersaturation decreases [12].

Large eddy simulations (LES) [41] obtained that the homogeneous mixing makes the spectrum expand near the top of the cloud, with a peak on the radius value quite high. As the inhomogeneous value increases, another peak begins to be generated for mean size values lower than the first peak, up to full homogeneous mixing, at which the spectrum where the main peak is at much lower radii than the homogeneous case is observed .The

formation of bimodal spectra observed in LES [41] (Figure 2.16) confirms what airborne measurements [18] had previously indicated, that is that entrainment produces bimodality in the observed measurement distributions.
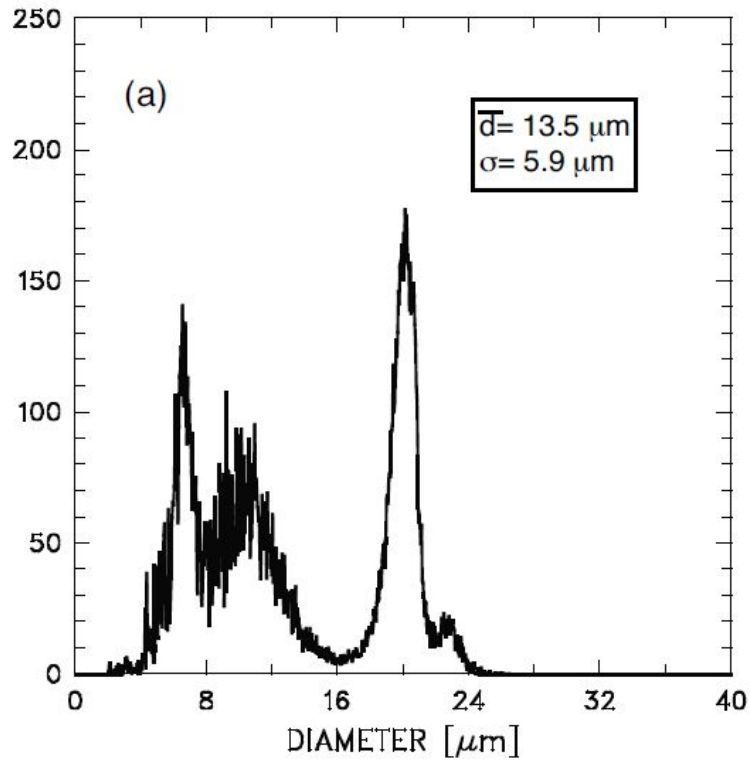
()

Figure 2.16: Calculated bimodal spectra [41]

Chapter 3

The radiosonde

As discussed in the previous chapter, the role of turbulence in cloud development and the onset of precipitation is still widely under discussion. This is because, although several studies have been carried out on the subject, the observations made in the field are still insufficient, and more precisely there is a lack of experiments that follow the turbulence from the Lagrangian point of view. In order to achieve this last point, one of the possibilities available is to make a radiosonde constituted by a balloon filled with helium. Previous experiments with balloons filled with helium have been carried out [42], but the size of the balloon was too large to follow the trajectory of the current faithfully.

COMPLETE (Cloud MicroPhysics Turbulence Telemetry) [2], an Horizon 2020 project, was therefore launched by the need to create an in-cloud Lagrangian database and to develop an inter/multidisciplinary network capable of improving current knowledge about the complex multi-scale natural phenomena taking place within the clouds.

One of the main tools with which COMPLETE intends to achieve its goal are in-situ experiments, using an innovative light, floating, economical, biodegradable mini-radioprobe. In order to obtain its main objective, the probe must attain 3 important goals:

- floating on an isopycnic surface at a chosen altitude of about 1000m for a time spanning from the inner turbulence (scale of minutes) to the extension of cloud lifetime (few days), using a balloon filled with helium;

- acquiring atmospheric data (pressure, temperature, humidity) and location data through the employment of sensors;

- processing and transmitting the acquired data to a ground station using a mini-antenna.

The balloon is filled with helium in order to obtain a buoyancy force equal to its weight, and the gas will have a pressure similar (or slightly lower) to atmospheric pressure at the designated altitude. The balloon volume, as will be shown below, will depend on the total weight of the probe and the height at which it will be released.

Atmospheric data will be captured through pressure, temperature and humidity sensors, in addition to movement sensors (accelerometer), which will capture data at regularly scheduled intervals [43].

Finally, the data will then be interpreted, processed, saved and transmitted through a micro-antenna to a ground receiver [44], [45].

3.1   Smart materials used for balloon

The material used to produce the balloon has to satisfy this following requirements [1]:

- **Not too elastic**, because the probe is designed to maintain its volume constant. If the material was too elastic, the gas inside it would tend to expand without problems. This is important to keep balloon weight constant;

- **Hydrophobic**, because water droplets in clouds would tend to adhere to the external surface of balloon, altering its weight. Through a hydrophobic material, this problem can be solved or at least contained;

- **Impermeable to helium**: the more *He* will leak out of the balloon, the more altitude of the probe will decrease. For this reason, the material must maintain gas when the balloon is fully inflated.

- As **cheap** as possible. Because its weight, the use of a GPS is not guaranteed and consequently, probes will not be recoverable. For this reason, several radiosonde will be produced, so the material should be easy to process and the cost need to be low.

- As **biodegradable** as possible. At the end of its life cycle, the balloons will be dispersed in the environment, so the material need to deteriorate easily.

- Finally, the material must guarantee a determined **inertia of temperature and relative humidity** between the inside and outside of the balloon: the sensors will be placed inside the balloon, so they may result insulated from atmospheric conditions and transmit incorrect data. To prevent this problem, the material must ensure that the temperature range ΔT and relative humidity range ΔRH are sufficiently low, with short transition times.

Several tests were carried out in laboratories of IIT (Italian Institute of Technology) [3], to test the characteristics mentioned above on two bio-degradable materials that are potential candidates for use in the production of the balloon: PolyLactic Acid (PLA) and Mater-Bi

To measure the elastic capacity of the materials, classic tensile strength tests have been carried out. To measure the hydrophobicity, it was obtained the *contact angle* of various materials, that is, considering a drop on a solid, the angle between the direction of the solid-liquid tension and the direction of the liquid-gas tension, tangent to the external surface of a drop, with the vertex at the three-phase liquid-solid-steam point (Figure 3.1). As the figure shows, the higher the contact angle value, the more hydrophobic the material can be considered.
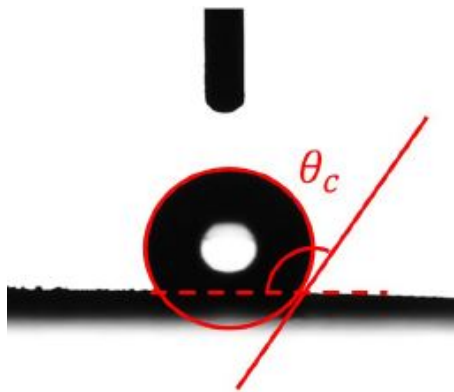

Figure 3.1: Example of contact angle of a drop of fluid on a solid surface

Finally, to assess the permeability of helium, balloons of different materials were filled and then placed on a scale: the velocity at which the weight of the balloon increases

determines the rate at which the helium is released from the balloon. Finally, to assess the difference in temperature and relative humidity between the inside and outside of the balloon, in [3] the balloons were placed, with the sensors inside, inside climatic chambers where certain values of ΔT and ΔRH can be chosen.

3.1.1 Coatings

Coatings have been applied to both PLA and Mater-Bi materials, in particular two solutions composed of Carnauba Wax + Pine resin and Carnauba wax + SiO_2 nanoparticles. For example, in the first case the solution was prepared with 0.5g Carnauba Wax + 0.5g Pine resin in 50g acetone, and then sprayed uniformly on the sheets of material before the balloon was built.

During the tests carried out in [3], coatings significantly improved material characteristics of interest. In particular, the most important improvements were seen in the hydrophobicity characteristics, represented by the contact angle value (Figure 3.2) and helium loss, represented by the weight gain of the balloon (Figure 3.3). On the other hand, for the other features, the improvements made have been more negligible.

Material	Mean contact angle [°]
Latex	79
Mylar	95
Mater Bi	89
Mater Bi+carnauba wax	125
Mater Bi+carnauba wax+Pine Resin	73
Mater Bi+carnauba wax+SiO_2 NPs	140
PLA	83
PLA+carnauba wax	126
PLA+carnauba wax+Pine Resin	81
PLA+carnauba wax+SiO_2 NPs	136

Figure 3.2: Contact angle for each of tested materials in [3]

Finally, it can be argued that the most suitable material for the construction of the radiosonde balloon is Mater-bi. This material is a bio-plastic of which the classic shopping bags are made, so it is cheap, easy to purchase and bio-degradable. Thanks to the coatings applied on this material, its characteristics improve considerably. In particular, the coating that includes silicon nanoparticles significantly increases the contact angle, as
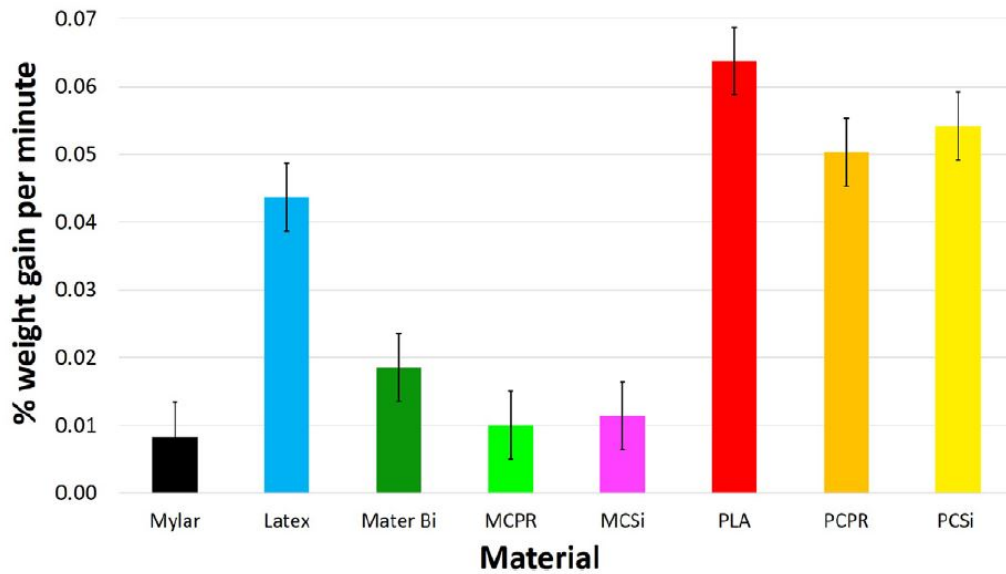
Figure 3.3: Weight gain per minute (dued to Helium loss) for each of tested materials in [3]

shown in Figure 3.2, which is very important because the balloon will fluctuate within the clouds, where the density of droplets will be very high and it should not raise its weight considerably.

3.2 Working principle

The operating diagram of the radio-probe is summarised in Figure 3.4.

The left part of the diagram in Figure 3.4 (marked in blue), is contained in the PCB (Printed Circuit Board) shown in Figure 3.5 , with dimensions of 5x5cm and weight of 7.5g, placed inside the balloon.

The right part of the diagram (orange blocks) consists of the ground station, in which the data receiver system is present; data will then be further processed and analyzed.

Therefore, the following components are arranged on the PCB [46]:

- a configurable set of **sensors**: pressure, temperature, humidity, 3-axial accelerometer.

    - Sensors for the **temperature** have a range from -10^oC to 40^oC and a resolution of at least 0.5^oC;
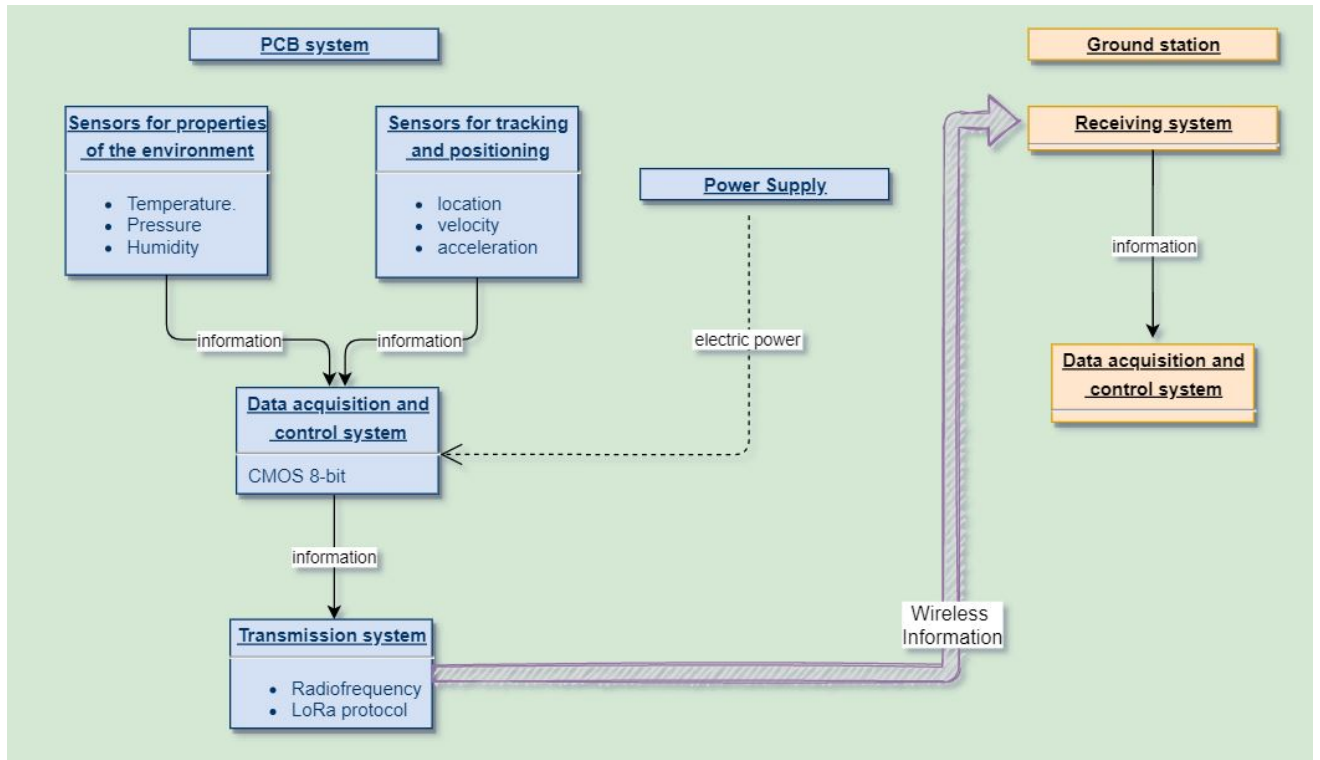
32

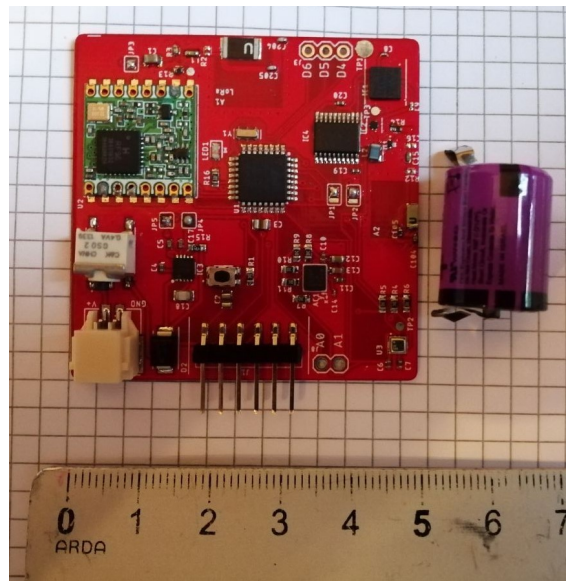Figure 3.4: Diagram of the radioprobe operation

Figure 3.5: PCB and battery used for the project

– Sensors for the **humidity** have a range from 0% to 100% and a resolution of
  at least 0.005%;

– Sensors for the **pressure** have a range from $400mbar$ to $1100mbar$;

SENSORS

BME280
Humidity, temperature
and pressure
Operating voltage:
1.71 to 3.6 V
Operating range:
-40°C to 85°C
Dimension: 2.5 x 2.5 x 1 mm
Weight: approx.: <0.5 gram

Diodes and transistors
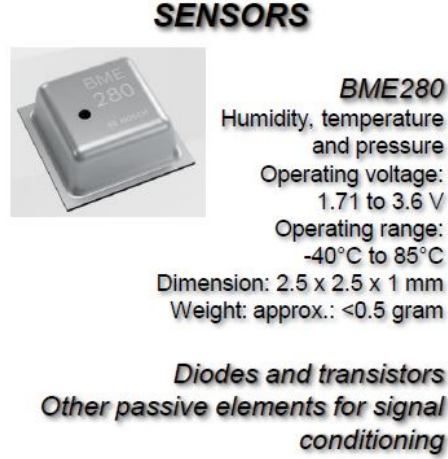**Other passive elements for signal**
conditioning

Figure 3.6: Humidity, temperature and pressure sensors [47]

– Sensors for the **trajectory** have a accuracy of about $+/-100mm$, a frequency rate smaller than 10Hz and a *total fluctuation* maximum of $20m/s$ inside clouds [47];

The sampling period for pressure, temperature and humidity is $T_{sensors} = 2s$, while the period for capturing trajectory is chosen to be $T_{accelerometer} = 0.1s$ [1].

To realize velocity and acceleration estimation, the chosen approach was radio signals combined with position estimation techniques to localize the target objects [47].

Since one single 1 three axial accelerometer is not enough to estimate position, and the radioprobes' constrains of weight and can be slightly modified, Inertial Measurement Unit(s) and/or a GNSS receiver could be incorporated to the design [47]. The use of a GPS to track in real time the probe has been temporarily excluded due to its excessive weight. This can however be considered for future versions.

• A single 4.0 V Lithium Metal Oxide (LMO) **battery** with nominal capacity of 125 mAh and pulse current capacity of 3.75 A is used, represented on the right in Figure 3.5. The battery, which measures $23mm$ of diameter, $5.4mm$ of height, $5.75g$ weight, has a nominal voltage of $3V$ and a nominal capacity of $500mAh$ [44]. The current consumption is estimated to be from $50mA$ without GPS, up to $100mA$ with the use of GPS. Consequently, according to such data, the evaluated duration

of the probe battery is from 5 to 25 hours, depending of the type of configuration.
[44]

- a **CPU** (CMOS8-bit), which forms the data acquisition and control system, where
  the data are pre-processed, saved and then transferred to the transmission module,
  to be sent to the ground. To keep the probe power consumption as low as possible,
  the micro-controller will maintain sensors in a sleep mode until they must perform
  a measure. Furthermore, the micro-controller will activate the transmission system
  when is required to transmit data to the ground receiver.
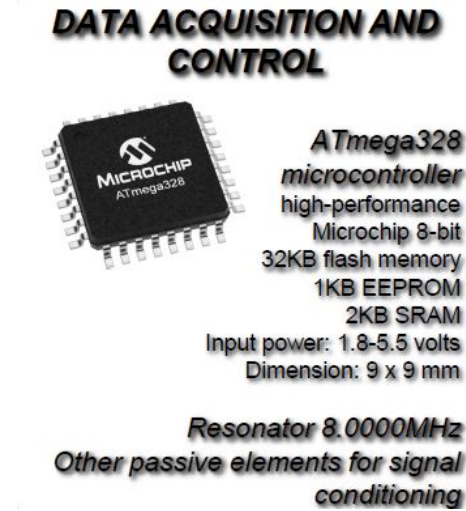
Figure 3.7: ATmega 328 microcontroller[47]

- An omni-directional **antenna** for data transmission to the receiver. Radio signals
  will be sent from the probe to a Earth receiver, using the frequency bands around
  350MHz or 169Hz. This permits to probe to be monitored at lower power dur-
  ing the entire flight through warm clouds because good propagation link and low
  attenuation are guaranteed.

  The signal is required to be received up to a distance of 20km, and the receiver has
  a sensitivity about $P_{receiver} = -130dBm$. Each probe must transmit a power of at
  least $P_{probe} = -30dBm$ if high gain 30dB antennas are used on Earth [45].

  The value that need more attention is probe power P_{probe}, because it is generated by
  on-board battery, which has a limited duration.

In order to obtain a simplified version to the highest degree, it was thought to reduce the whole system to a constant frequency emitter (e.g. 350MHz). The receiver on Earth would have been able to reconstruct the range of velocity fluctuations due to turbulence thanks to the Doppler effect: a velocity variation of 1m/s in the field produces a frequency shift equal to 1Hz [44]. The equation from which the velocity would be derived is:

$$F_d = f \cdot \frac{v}{c} \tag{3.1}$$

where F_d is the *Doppler frequency*, c is the light speed [48].

However, a more complex receiver is needed since transmitter is equipped with a set of sensor. In this case, no Doppler analysis is required because the probe position and velocity can be established using the IMU and GNSS data. Furthermore, it is needed to exploit also RSSI (Receiver Strenght Signal Indicator) algorithm and positioning techniques [44].
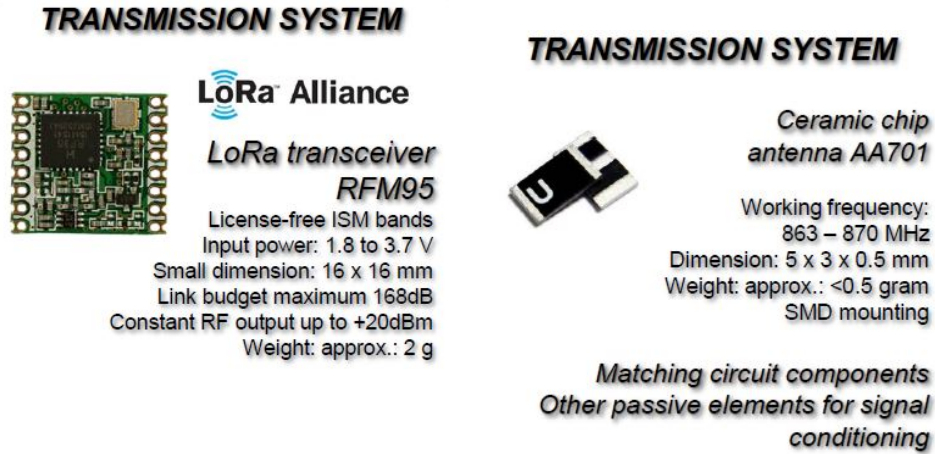

Figure 3.8: Components of transmission system: LoRa transceiver [45] and micro-antenna[47]

3.2.1 Turbulence study techniques

To achieve a detailed study of the evolution of clouds and therefore of precipitation, it will be necessary, eventually, to implement an experimental method through numerical, laboratory and in-field investigations. For this reason it will be useful to generate turbulent flows, saturation fields, CCNs and water droplets, both in the laboratory and in numerical simulations, through the steps below:

- monitoring the growth of droplets, so their diameter, is used the *Phase Doppler Particle Anemometry*;

- observing the collision between droplets are used the *Particle Tracking Technology* and the *Planar Laser-Inducted Fluorescence (PLIF)*;

- measuring particle concentration and size distribution are used *LIDARs* and *Mini Wide Range Aerosol Spectrometers*;

- monitoring the concentration of water vapor through a *Microwave Radiometer (MWR)*.

Chapter 4

Balloon assembly

4.1 Target

The aim is to create a probe capable of floating on an isopycnic level in the clouds, which follows the trajectories of the current in a Lagrangian way and captures turbulent fluctuations, as well as collecting data on pressure, temperature and relative humidity for at least an hour.

To guarantee the aimed stability and precision in fluctuation reproduction, the balloon must be as spherical as possible, and the PCB (printed circuit board) which contains sensors and battery must remain as much as possible in the centre of the balloon, in order to avoid undesirable oscillations.

Obviously, during the following procedures the air density at sea level has been considered, since the part of the experiment described here takes place in the laboratory under environmental conditions.

4.2 Preventive estimations

Before proceeding with the physical construction of the balloon, it is necessary to realize an estimate of the volume of helium necessary for the probe to remain suspended.

To achieve this result, it is necessary to know the total weight of the structure, which will be the sum of the PCB, the battery, any structure necessary to hold the sensors in the centre of the balloon and finally the weight of the outer casing (Mater-Bi).

However, in order to be suspended, the probe *overall weight* (W_{tot}) must be balanced by the *hydrostatic thrust* ($H.T$) that the helium makes upwards, hence:
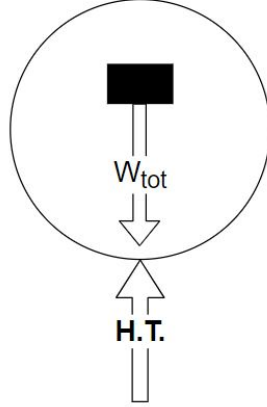
$$H.T. = W_{tot} \tag{4.1}$$

Figure 4.1: Forces equilibrium of a ballon filled with Helium in atmospheric air

Where the overall weight is given by:

$$W_{tot} = M_{tot} \cdot g \tag{4.2}$$

A volume, containing a lighter fluid (ρ_{He}) than that in the external environment (ρ_{air}), generates a hydrostatic thrust:

$$H.T. = Vol \cdot g \cdot (\rho_{air} - \rho_{He}) \tag{4.3}$$

Hence, equating:

$$Vol \cdot g \cdot (\rho_{air} - \rho_{He}) = M_{tot} \cdot g \tag{4.4}$$

For this reason, the Helium volume (Vol) necessary to keep the probe in suspension is given by the following equation:

$$Vol = \frac{M_t}{\rho_{air} - \rho_{He}} \tag{4.5}$$

Because the density value of a gas is dependent on the conditions under which it operates according to the law of perfect gases

$$\rho_{gas} = \frac{pM}{RT} \tag{4.6}$$

the volume formula should be modified as follows to make it more easily applicable to changing environmental conditions

$$Vol = \frac{M_t}{\rho_{air}\left(1 - \frac{M_{He}}{M_{air}}\right)}$$ (4.7)

having considered the equal conditions of pressure and temperature between the inside and outside of the balloon. $M_{He} = 4,003$ and $M_{air} = 28,96$ are the molecular weights of helium and air respectively.

Depending on the altitude, therefore, a different volume will be required as the air density decreases with increasing z, as shown in Figure 4.2. During the first phase of the tests the density considered is $\rho_{air} = 1.225 kg/m^3$, since the attempts are carried out inside the laboratory.

Z [m]	T [K]	P $\times 10^4$ [Pa]	ρ [kg/m³]	μ $\times 10^{-5}$ [kg/ms]
0	288	10.0	1.22	1.79
500	285	9.5	1.17	1.78
750	283	9.3	1.13	1.77
1000	282	9.0	1.11	1.76
1250	280	8.7	1.08	1.75
1500	278	8.5	1.06	1.74
2000	275	7.9	1.01	1.73
3000	269	7.0	0.90	1.70

Figure 4.2: Relationship between altitude and air characteristics

Finally, if we approximate the balloon as perfectly spherical balloon, we can simply obtain the diameter:

$$d = 2 \cdot \left(\frac{3}{4} \cdot \frac{Vol}{\pi}\right)^{\frac{1}{3}}$$ (4.8)

The measurement of the circumference is important because it is used as a reference during the assembly of the balloon:

$$c = \pi \cdot d$$ (4.9)

as it inflates, the diameter changes because of the third dimension, while the external circumference remains the same.

4.2.1 Balloon dimensions

In order to estimate the size of the balloon, it is necessary to know or estimate the weights of the components that will fluctuate. While PCB and battery are unvarying weights, the weight of the outer case is highly dependent on the size of the balloon. In fact, the weight of the outer case can only be established with certainty once the balloon has been built.

One way to determine the weight of the external balloon could be to proceed by iteration:

- initially calculation of the volume and then the radius needed to fly the balloon, without inserting the weight of the outer case

- realization of a balloon with the calculated dimensions;

- weighing the deflated balloon which has just been made, obtaining the weight of the outer case: now it is known the minimum weight that it can have.

- estimation of the size of the next balloon by estimating an arbitrary increase (about 0.5g) in the weight of the outer case;

- proceeding until an equilibrium is reached.

The structure useful to keep the PCB in the centre of the sphere, on the other hand, was easier to calculate and weighs 2g. Below is a summary table with the weights of the components that form the probe.

	Weight [g]
PCB	7.5
battery	10
outer case	9.5
additional structures	2
Overall weight	29

Given the overall mass, we can now conclude that the downward thrust will be equivalent to:

$$W_{tot} = M_{tot} \cdot g = 0.029 kg \cdot 9.81 \frac{m}{s^2} = 0{,}28449 N \qquad (4.10)$$

And consequently the hydrostatic thrust that the balloon will have to exert will be exactly:

$$H.T. = W_{tot} = 0{,}28449N \tag{4.11}$$

The volume of helium needed to generate this thrust must therefore be equal to:

$$Vol = \frac{M_t}{\rho_{air}\left(1 - \frac{M_{He}}{M_{air}}\right)} = 0{,}02747m^3 \tag{4.12}$$

As already described, the air density value used is the one at sea level ($\rho = 1{,}225kg/m^3$). It is necessary to change this value since the balloon is aimed to float at a different altitude (Figure 4.2).

The diameter of the balloon must hence be:

$$d = 2 \cdot \left(\frac{3}{4} \cdot \frac{Vol}{\pi}\right)^{\frac{1}{3}} = 0{,}3743m \tag{4.13}$$

Finally, the circumference corresponds to:

$$c = \pi \cdot d = 1{,}1754m \tag{4.14}$$

4.3   Instrumentation

The tools needed to assemble the balloon are shown below:

- Bags of Mater-Bi with thickness film of about $30\mu m$, available in any supermarkets/hygiene shops;

- a surgical scalpel/ scissors to give the desired shapes to the sheets of material;

- a ruler of about 60cm;

- a pen or a marker;

- a *hand wheel sealer* with heated wheel connected to a handle (Figures 4.3 and 4.4);

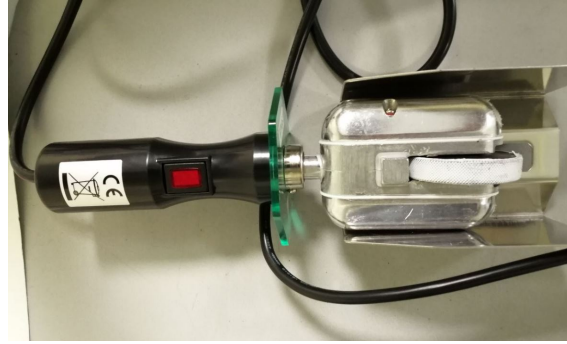- a Teflon tape to be applied on the heated wheel;

Figure 4.3: Welding machine

Figure 4.4: Technical characteristics of the sealer (a) and control knob to adjust the temperature(b)

- a sheet of rubber that prevents damage to the table, and a sheet of Teflon that impedes the Mater-bi and the rubber from adhering to the table;

- a 99% of pure helium tank with straw to inflate the balloon and a pressure gauge;

4.4 Assembly

The aim is therefore to obtain a final shape that is as spherical as possible, but without excessively complicating the structure of the balloon. In fact, Mater-Bi is a very delicate material, so it is likely that holes will form that would compromise the experiment. For this reason, it is advisable that the balloon is composed of as few pieces as possible, and that it does not contain critical points where numerous seams converge.

To facilitate the inflation of the balloon, it was necessary to provide an inlet for the straw that leads the helium from the tank to the balloon. The solution, as shown in more detail below was to set up a hollow protuberance into which to insert the straw

As for the structure that ensures the PCB remains in the exact centre of the ball, the solution had to be as light and simple as possible. The solution finally adopted was to create a pocket entirely of Mater-Bi in which to insert the board. The pocket is then soldered onto a band, also made by Mater-Bi, which in turn is anchored to two ends of the balloon. In other words, the band follows the diameter of the sphere, with the PCB in the centre of it.

4.4.1 Procedure

The following procedure shows the measures necessary to produce the balloon of the dimensions described in subsection 4.2.1, that is:

Volume	$0,02747m^3$
diameter	$0,3743m$
circumference	$1,1754m$

1. Connect the *hand wheel sealer* to the socket and set the temperature to 60^oC using the appropriate regulator (Figure 4.4b). It requires 15-20 minutes to reach the optimal temperature. It is necessary to pay a lot of attention to the use of this machinery: after reaching the optimal temperature of about 60^oC, it continues to overheat and after a certain period of time (about 20 minutes) it can reach temperatures so high it may destroy the material with which it is working. It is therefore advisable to switch off the hand wheel sealer for about 3 minutes every 15-20 minutes of use, in order to allow it time to cool down. Anyway, before carrying out an important welding operation, always perform a small test on waste material to evaluate the performance and temperature of the instrument.

2. Build two discs of Mater-Bi with a diameter of $0.60m$:

   - Cut the seams of two bags with the scalpel and open them in two sheets (sheet A and sheet B).

   - If the just created sheets are not sufficiently wide to draw two $60cm$ circles, you will need to start from 4 sheets: A1, A2, B1, B2 to create sheets A and B respectively.

This can be done by overlapping sheets A1 and A2 and passing with the *hand wheel sealer* on one side. At this point a single large sheet A with a seam is obtained. Repeat the same procedure with sheets B1 and B2 to obtain sheet B.

- With the help of the ruler and the marker, draw the circle with a diameter of $60cm$ on sheet A.

- Draw a rectangle of about 5cmx20cm that comes out of the circle, which will be used to inflate the balloon (Figure 4.6).

- Overlap sheet B on sheet A, trace the shape first with the marker pen (the sheets are semi-transparent), and then follow the outline with the scalpel.

3. Construction of the central band containing the PCB.

- From the waste, cut out a long strip of about 5cmx70cm, and two squares of 10cmx10cm.

- Place the PCB between the two 10cmx10cm squares previously cut out and seal the contours to close the board inside this pocket. Leave the upper input free to connect the battery to the last one before flight.

- at 19cm from one end of the 5cmx70cm tape weld the newly created pocket, as represented in Figure 4.5.
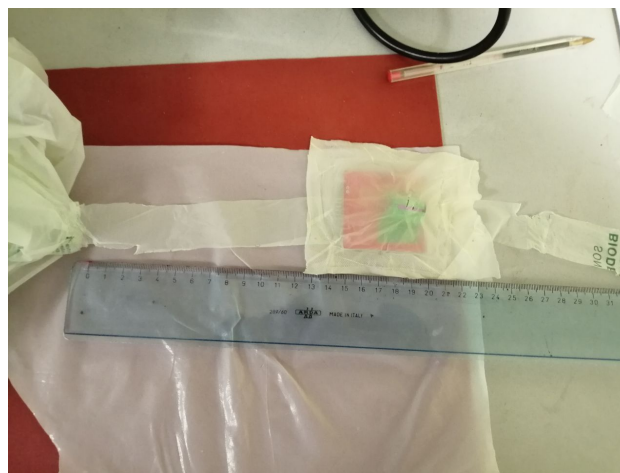
Figure 4.5: Central band containing the PCB

- Position the newly created structure between the two previously constructed discs so that the strip containing the PCB passes through the entire diameter, as shown in the illustration 4.6. The extremity of the short section of the strip
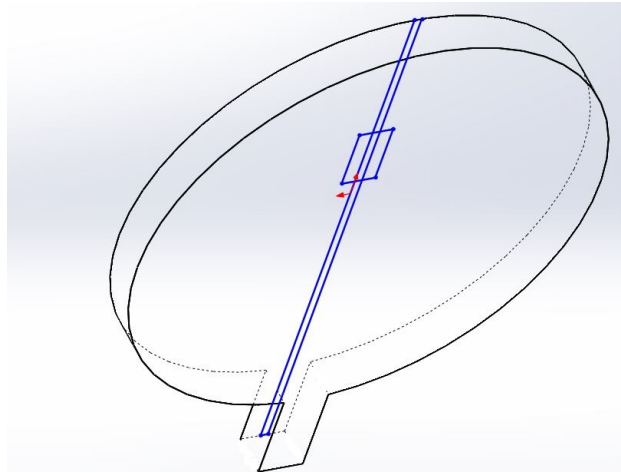

Figure 4.6: Scheme of application of the structure containing the PCB between the two discs that will compose the balloon

must be welded to the head of the balloon, while the long side must come out of the balloon.

4. Weld the two discs together with the *hand wheel sealer* following their contour. Leave un-welded the lower entrance of the rectangle (where the helium will enter) and about 10 centimetres of your choice along the perimeter .

5. Pass the PCB strip through the inlet of the straw. The long ribbon must exit the balloon through the helium inlet.

6. Insert the hand into the opening left to allow the pcb pocket to come out, connect the battery, close (by welding) the PCB pocket, replace inside the pocket and close the external opening. The balloon is now ready to be inflated.

7. Fill slowly with helium, using the appropriate knobs (Figure 4.7), until the balloon is inflated enough to push upwards. If it is inflated with excessive pressure, the balloon tends to develop small holes, dangerous to the success of the experiment. Remove the helium straw.

Figure 4.7: Filling with helium and knobs

8. Pull the ribbon until the PCB is in the centre of the balloon, but apply pressure at the inlet so that the gas does not escape.

9. Weld the balloon inlet and cut the excess ribbon.

Chapter 5

Data obtained from experiments

Several tests have been carried out to prove the instrumentation developed up until this moment. Following are preliminary tests, so the data may not be completely reliable or incomplete.

Prior to the tests defined as more complete in the following sections, other experiments were carried out to assess the reliability of the response of the various components.

A test was initially performed to evaluate the performance of the position sensors. A walking path was then taken by a user who was holding a working probe and a mobile phone capable of recording the position, to make a comparison. The results, which can be defined as satisfactory, are shown in the images below (Figure 5.1 and 5.2)

Figure 5.1: Pathway reported by the two devices
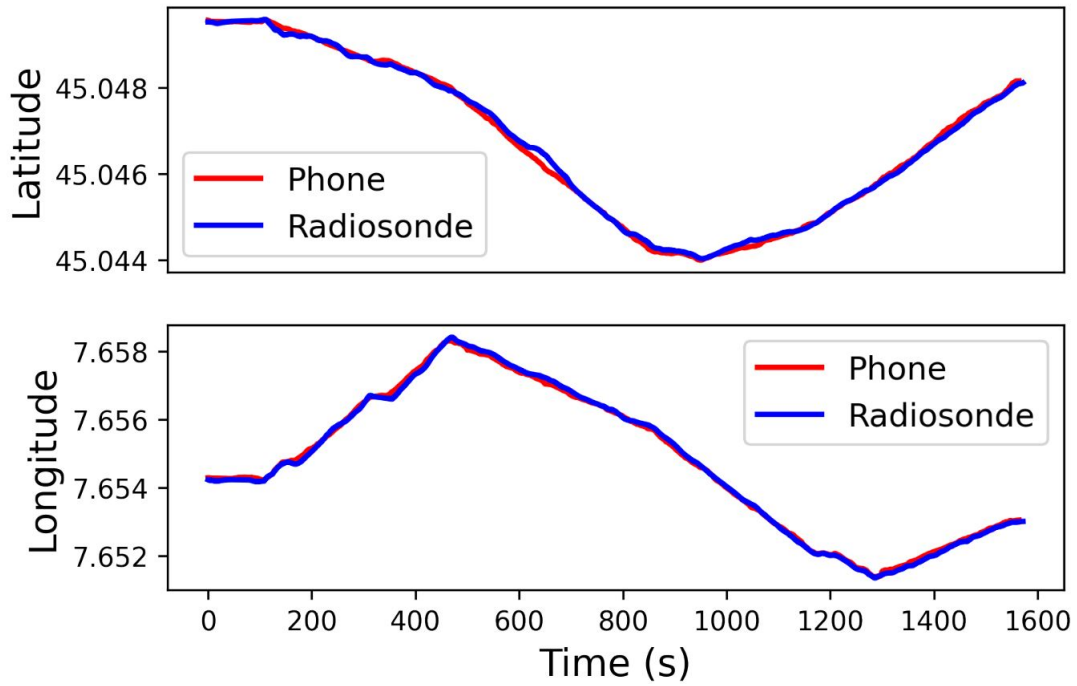
Figure 5.2: Comparison of the position detected by the two devices

A test was then carried out in which the PCB was attached to a remote-controlled drone and transmitted information, including pressure, temperature, humidity, from different altitudes. The results are not reported because they were unsuccessful and unreliable, due almost certainly to the interference that the very delicate sensors on the PCB received from the vibrations coming from the UAV.

5.1 Envisens Balloon tests

The experiments in this section were carried out near the Levaldigi airport, using an atmospheric balloon belonging to Envisens, considerably larger than the one in our project. Inside was placed the COMPLETE PCB, as well as sensors of the Vaisala probe. For this reason, it was easy to make a comparison between the data coming from the two sensors.

The PCB was anchored to the balloon by a string and using a support, as shown in Figure 5.3. The following figures show the comparison between the results coming from the two different probes carried by the balloon. In particular, the position data are given by GPS in the form of coordinates in degrees, then transformed into distance in meters for better readability.

49
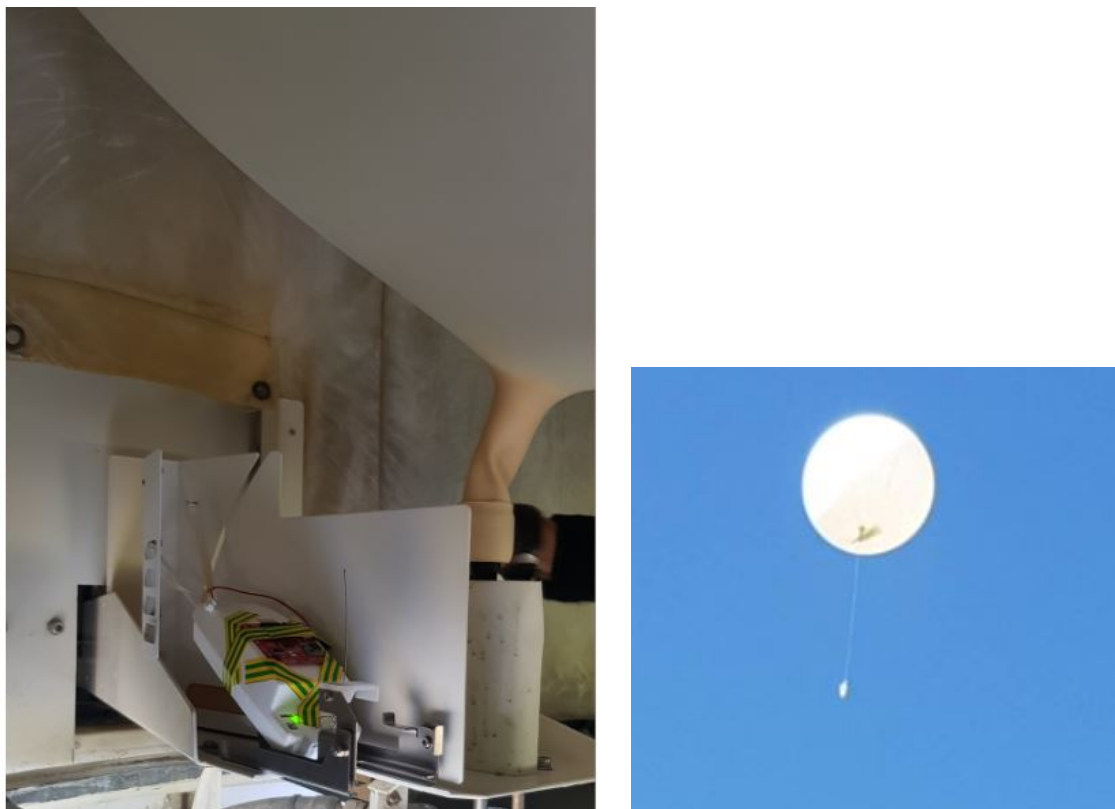
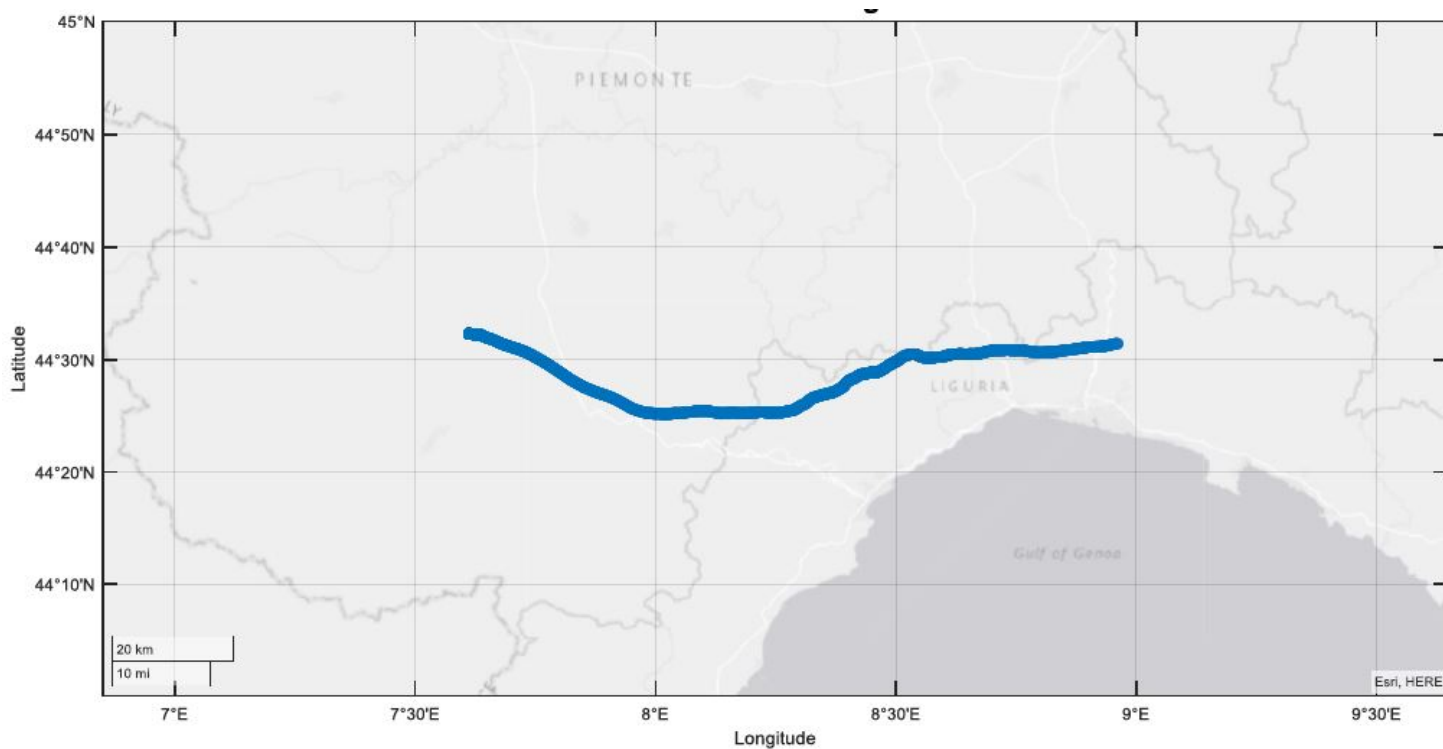Figure 5.3: Installation of the probe on the balloon

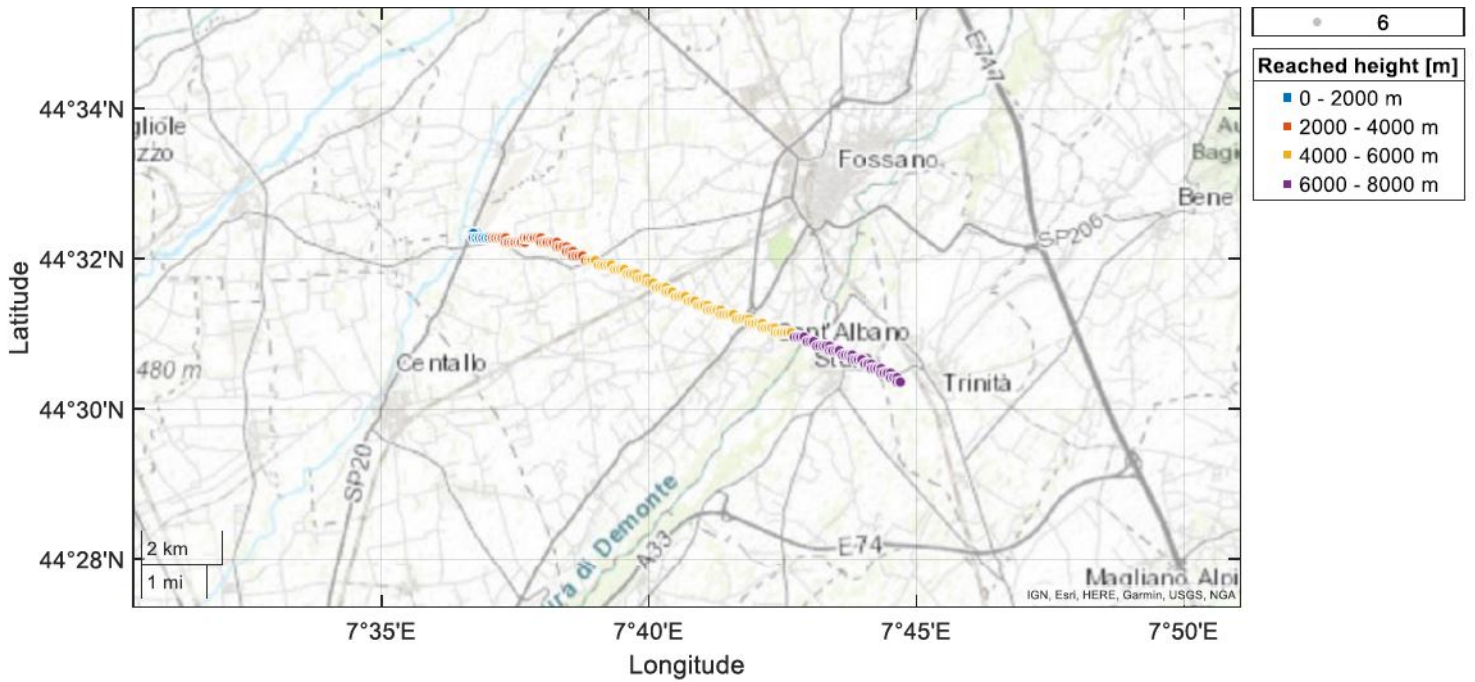Figure 5.4: The balloon path reported by the Vaisala probe is shown here

Figure 5.5: Radioprobe displacement. Our probe was able to transmit up to over 7km in height, and almost 12km in horizontal distance, for a total distance of 14km
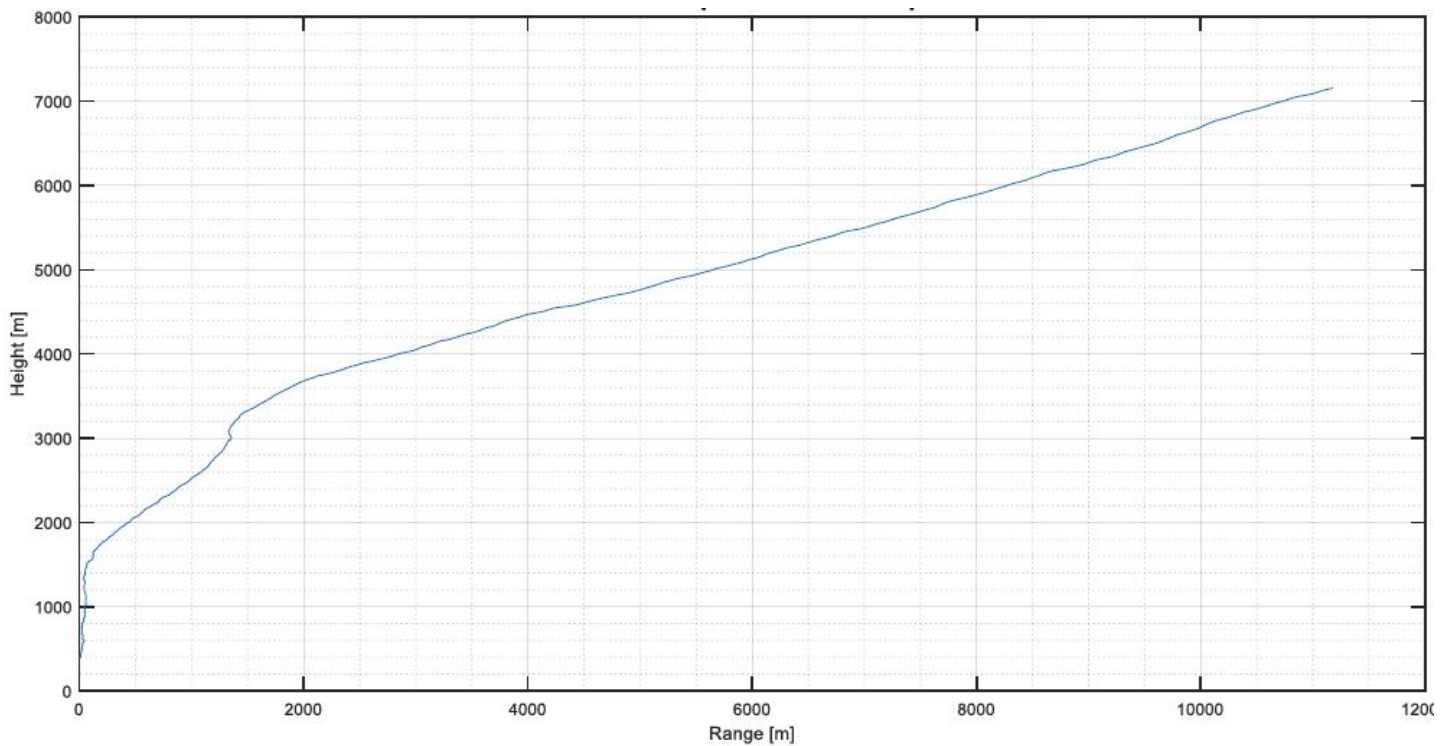

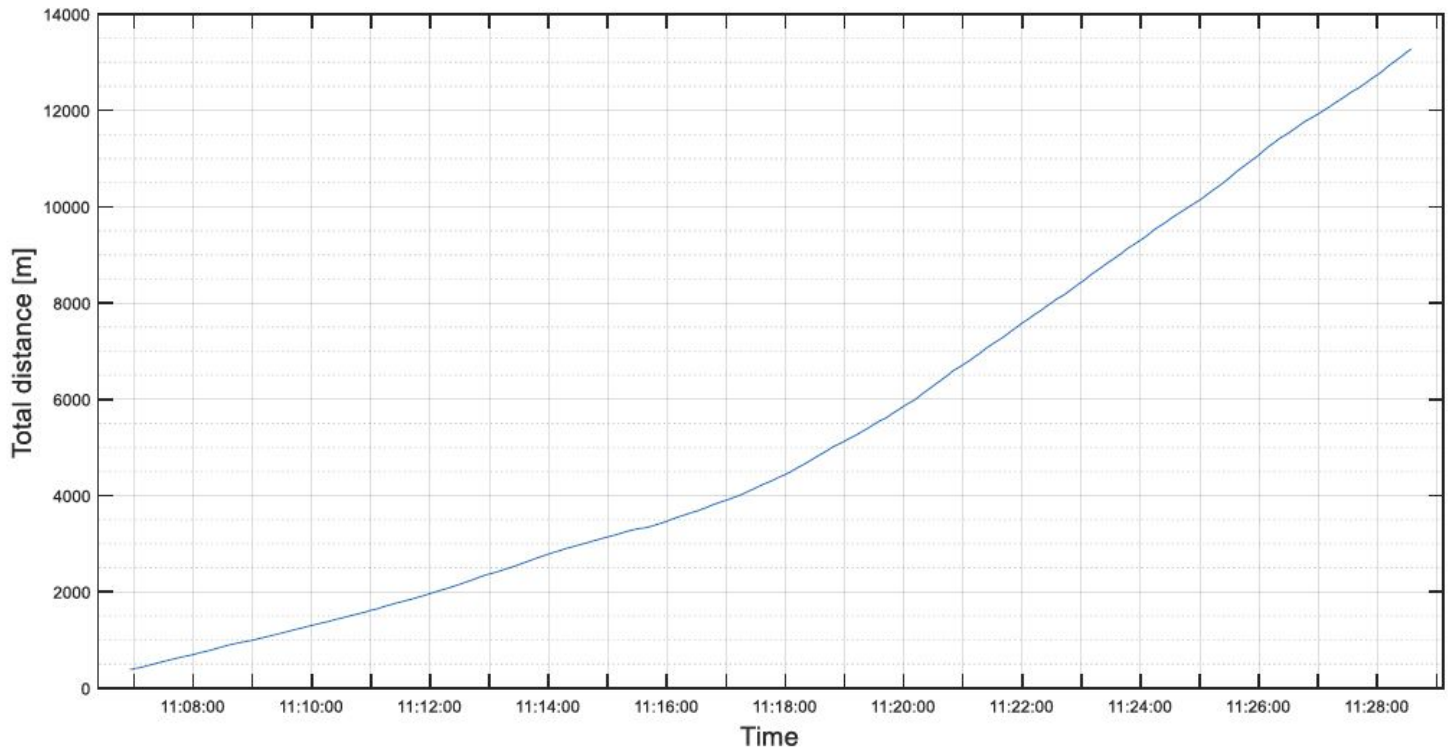Figure 5.6: Total travelled distance

51

Figure 5.7: Total distance reached by the radiosonde, after 30 minutes of transmission
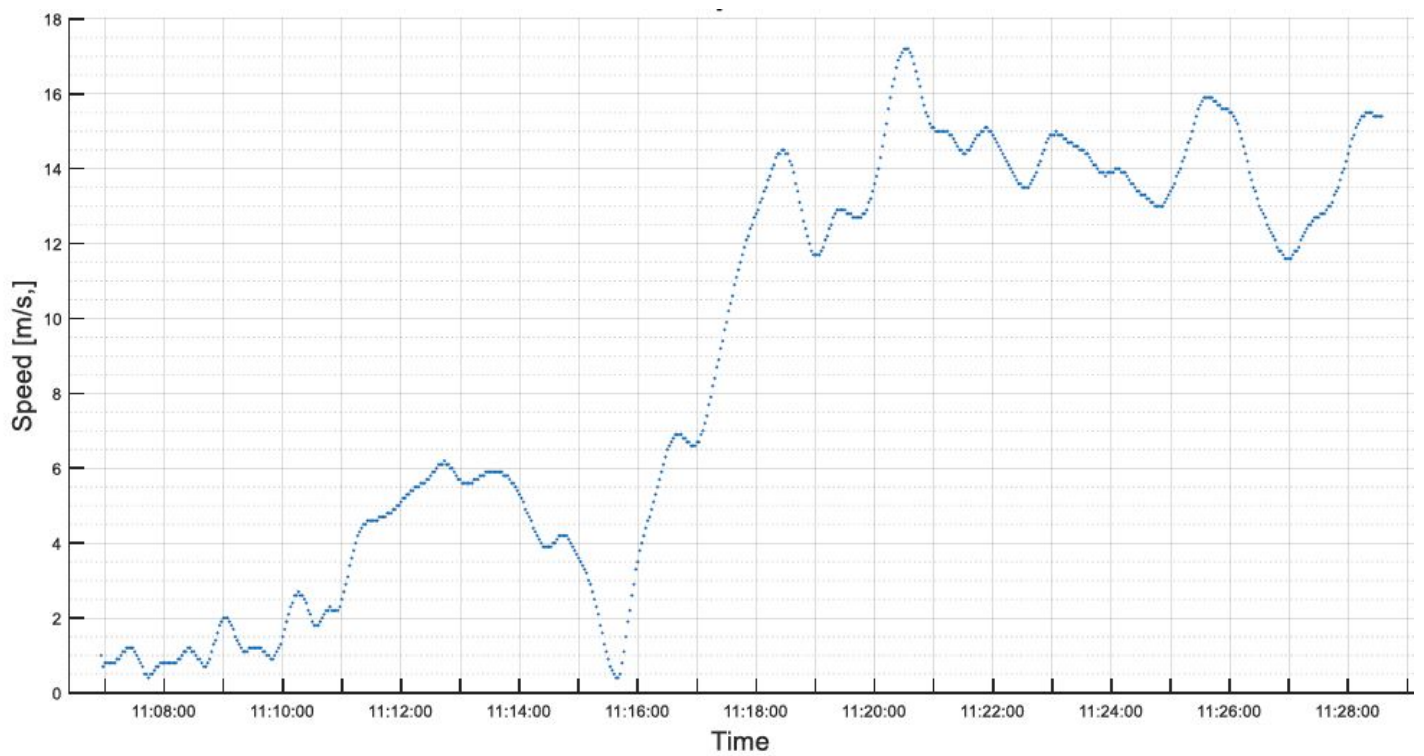

Figure 5.8: Speed variation as a function of time during radiosonde flight
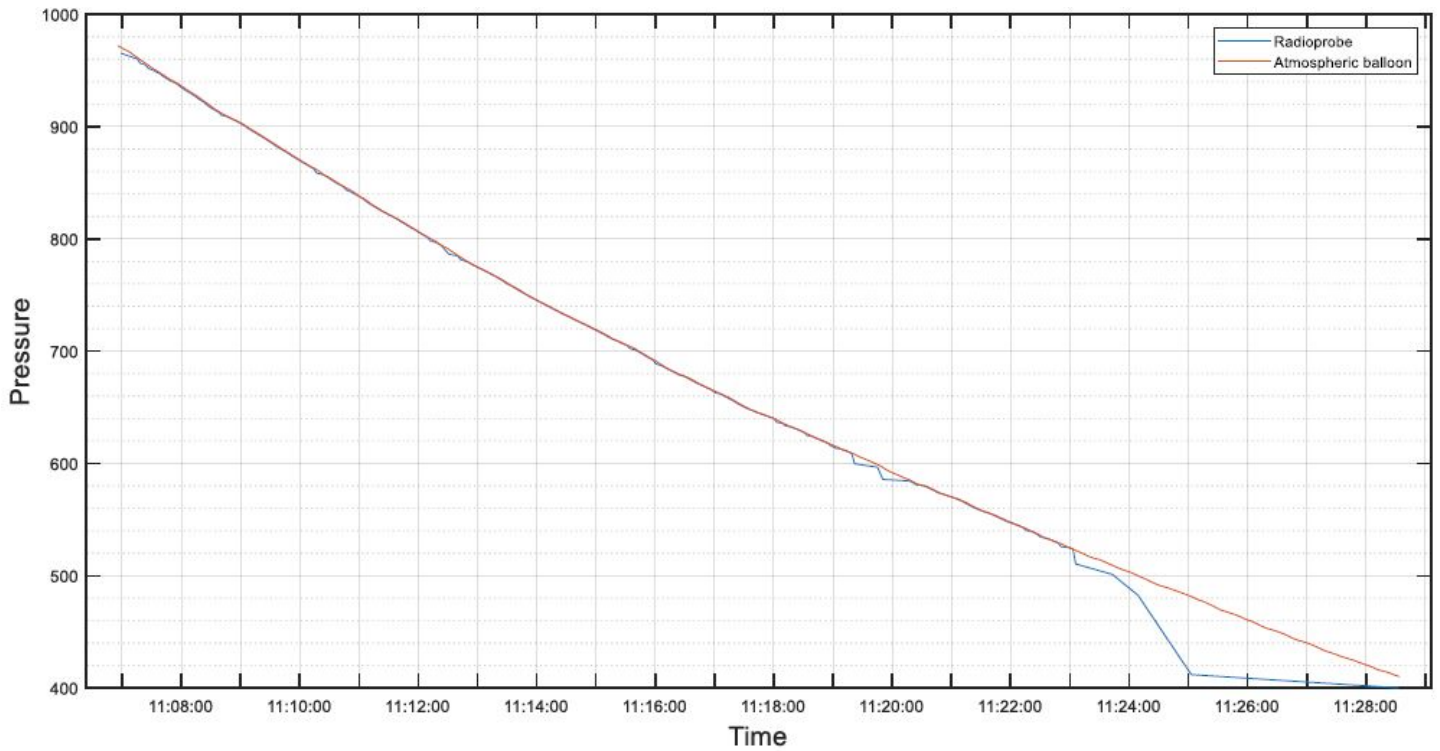
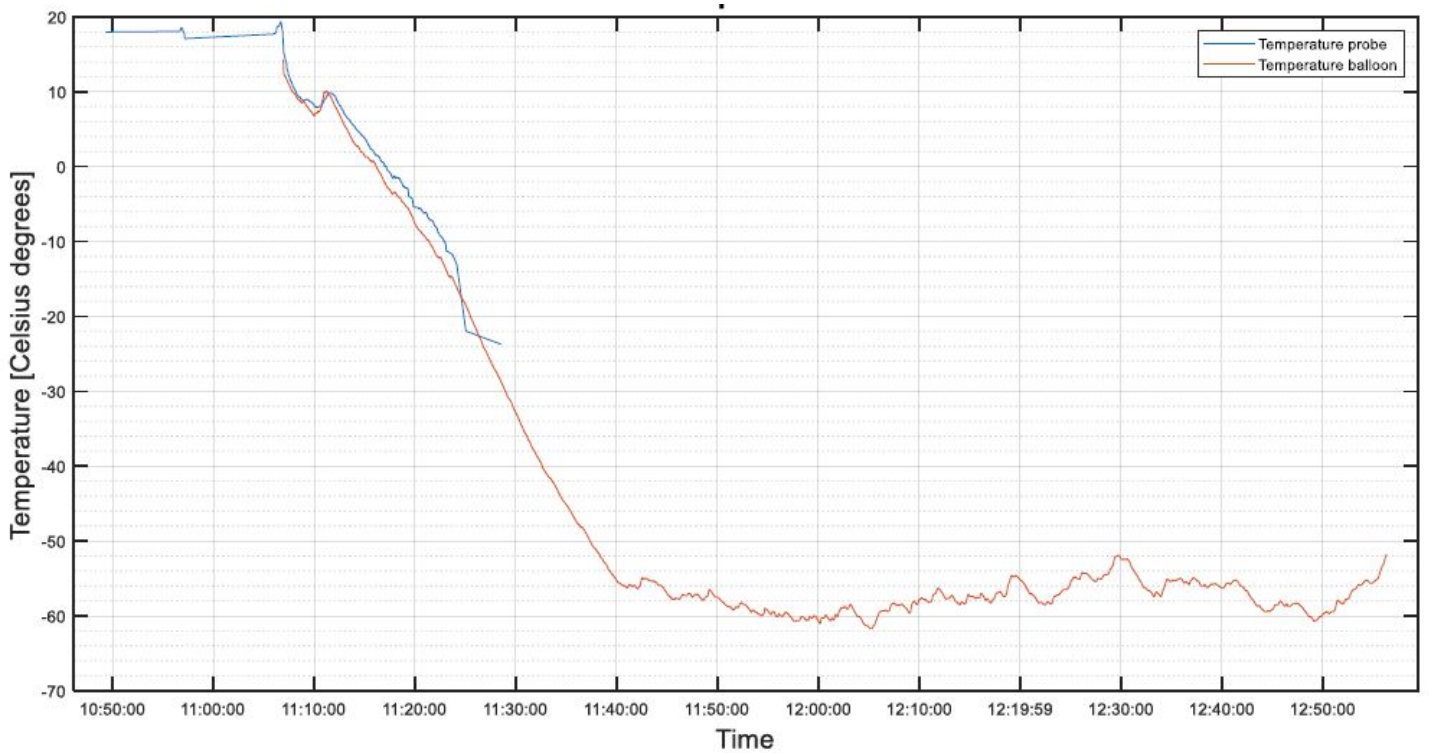Figure 5.9: Pressure variation as a function of time during radiosonde flight

Figure 5.10: Temperature variation as a function of time during radiosonde flight, with a focus on period when the radiosonde transmitted
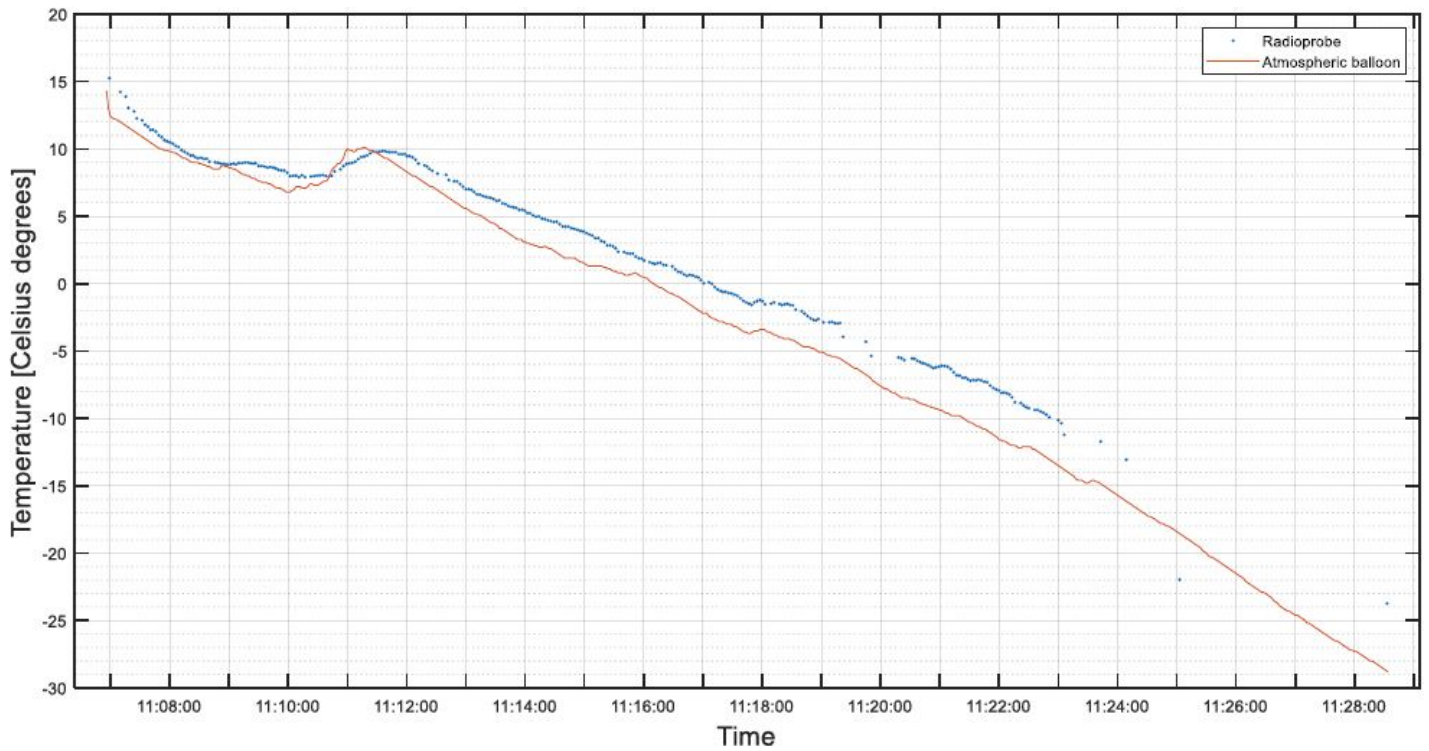
53

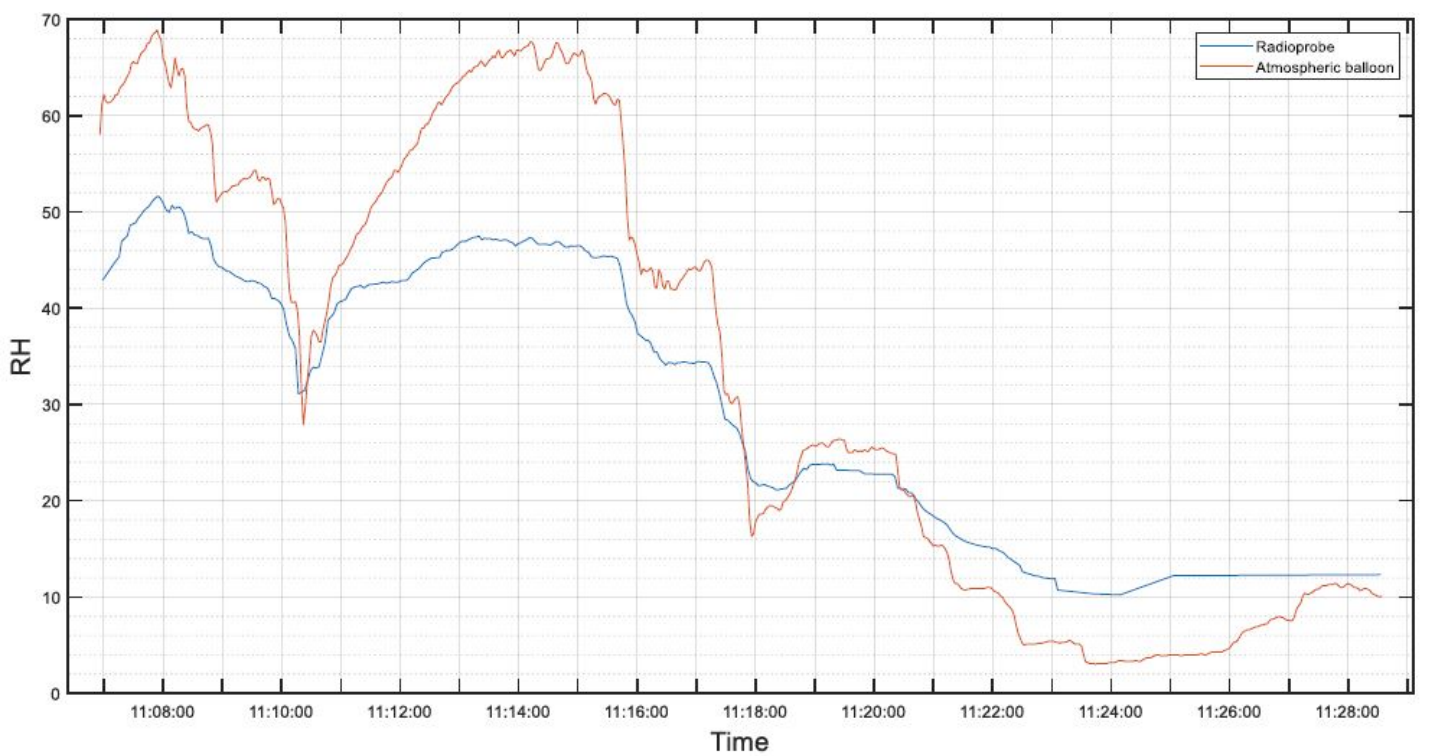Figure 5.11: Temperature variation as a function of time during radiosonde flight

Figure 5.12: Relative humidity variation as a function of time during radiosonde flight

5.2 COMPLETE Balloon test

The experiment described in this section wanted to test the COMPLETE project radio-probe as a whole: the developed electronic components were placed inside the balloon realized by the undersigned in the IIT laboratories, with the technique developed and explained in Chapter 4. The test mentioned in this section was carried out near a park on the outskirts of Turin, on 9 November 2020, on a clear day. Obviously, being the first in-field test carried out for the balloon, several initial difficulties were encountered, however they were overcome. A 20l portable helium cylinder was used.

The main difference to what will be the most valid tests in the future is that the balloon was tied to a cord so that it could not be dispersed. This has made it possible to carry out the tests on data transmission and the effectiveness of the balloon, but without wasting components that can be used for better tests in the future.

The radio-probe fluctuated for over 20 min, after which it was brought down as it had finished transmitting data due to low battery charge. The battery life is about one hour, but the first 30 minutes were lost due to technical problems with the above mentioned assembly.

The data was transmitted to the ground receiver at 3-second intervals and the initial time intervals from when the sensors in the PCB were activated to the moment the balloon was actually floating were excluded from the graphs for greater readability.

5.2.1 Data from positioning sensor

The latitude and longitude data were transmitted by the probe in the form of coordinates in degrees. In order to create a more readable chart, the starting point and reference system for the two directions was chosen as the location where the probe was at the moment it started transmitting valid data, that is:

- longitude:$7^o62'51,008''$

- latitude: $45^o01'26,520''$

- altitude: $29,8045m$

Furthermore, in order to better understand the information, it is important to point out that the direction module is towards the North for the direction corresponding to latitude and towards the East for the direction corresponding to longitude. For this reason, values with positive modulus in Figure 5.13 are positive in the East direction and negatives in the West direction; likewise, values in Figure 5.14 are positive when they are further North than the initial reference point.

Finally, in Figure 5.16 the movement of the probe was represented ignoring its vertical displacement, showing the various points where it transmitted the radiosonde without considering the height variations.
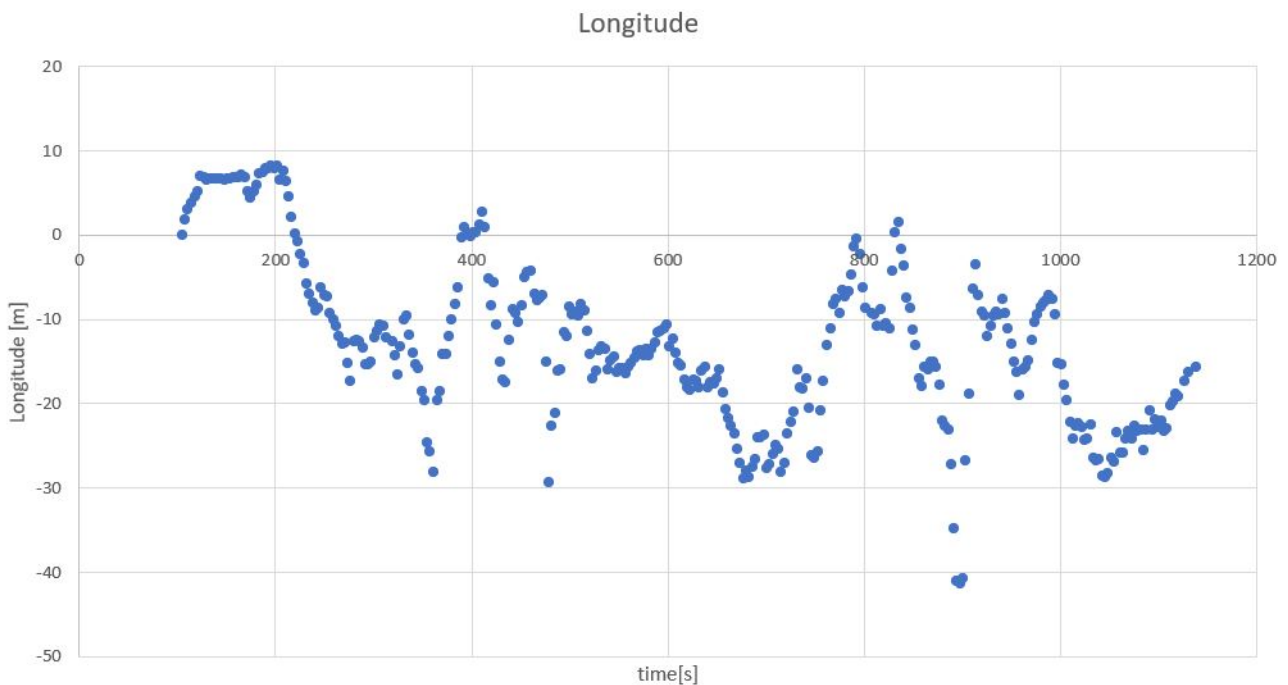

Figure 5.13: Diagram showing the movement of the probe along the longitude direction during the time fluctuation. As already written above, the negative longitude values indicate that the balloon tended to move further West than the initial point due to the wind
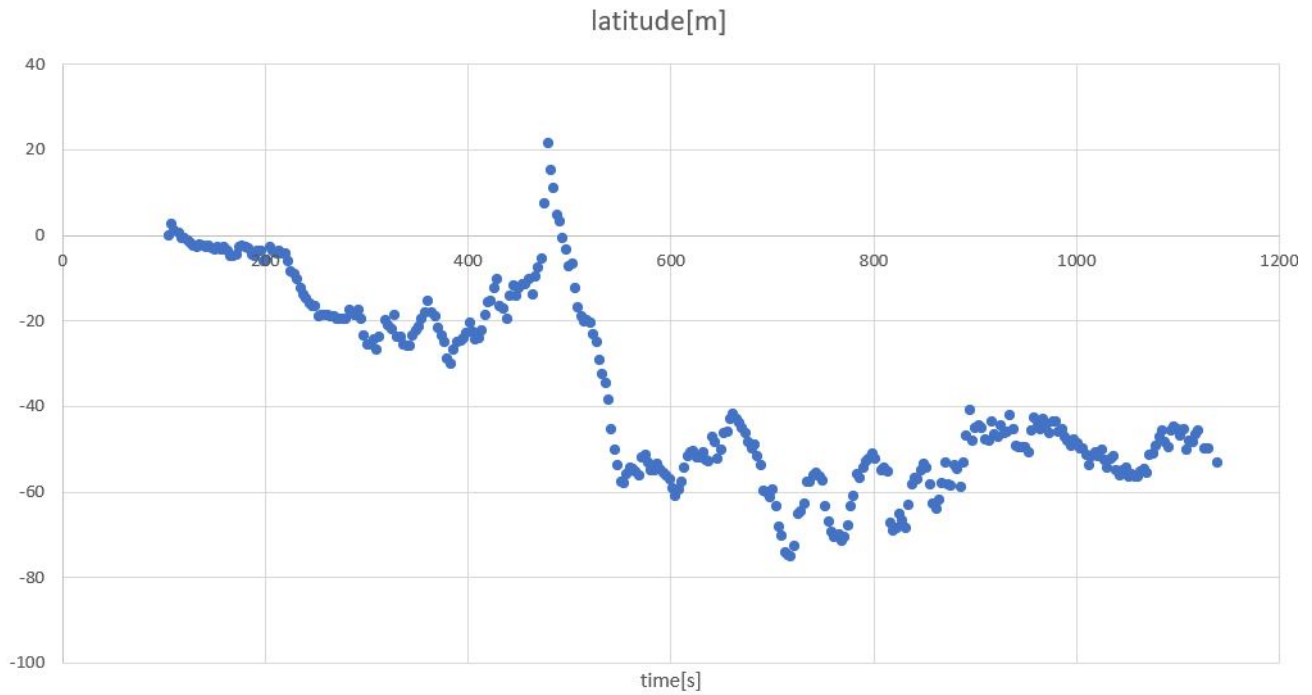
Figure 5.14: Diagram showing the movement of the probe along the latitude direction during the time of fluctuation. As already written above, the negative longitude values indicate that the balloon tended to move further South than the initial point due to the wind
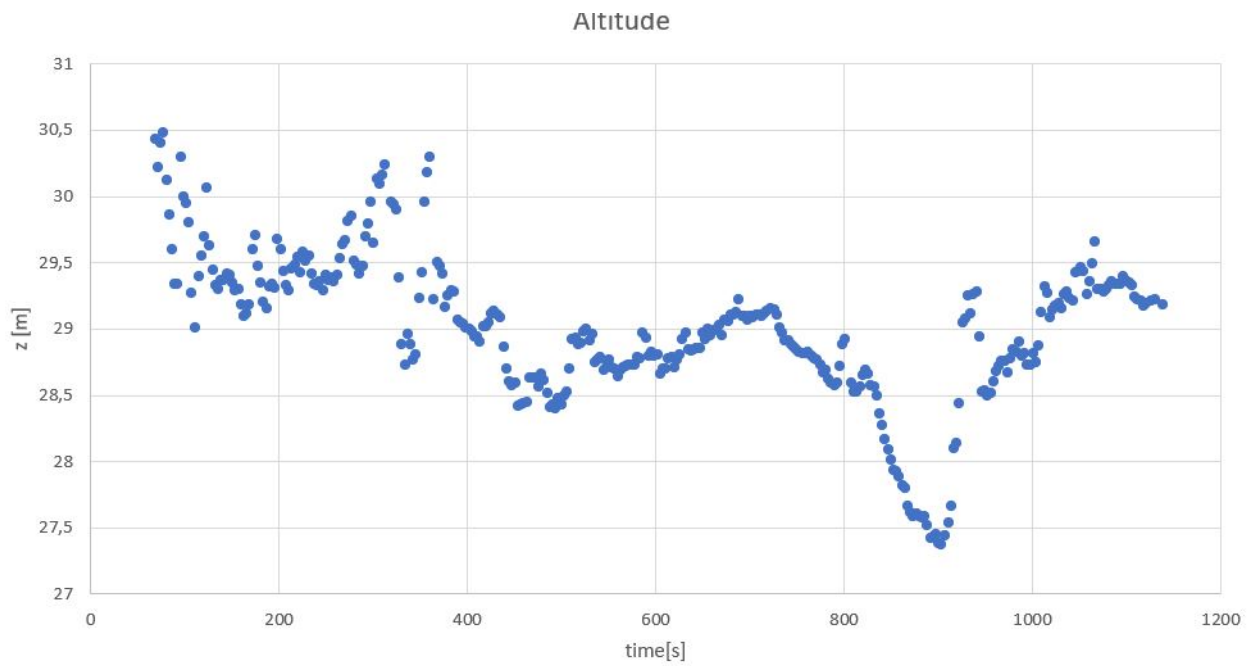

Figure 5.15: Diagram showing the movement of the probe along vertical direction during the time fluctuation
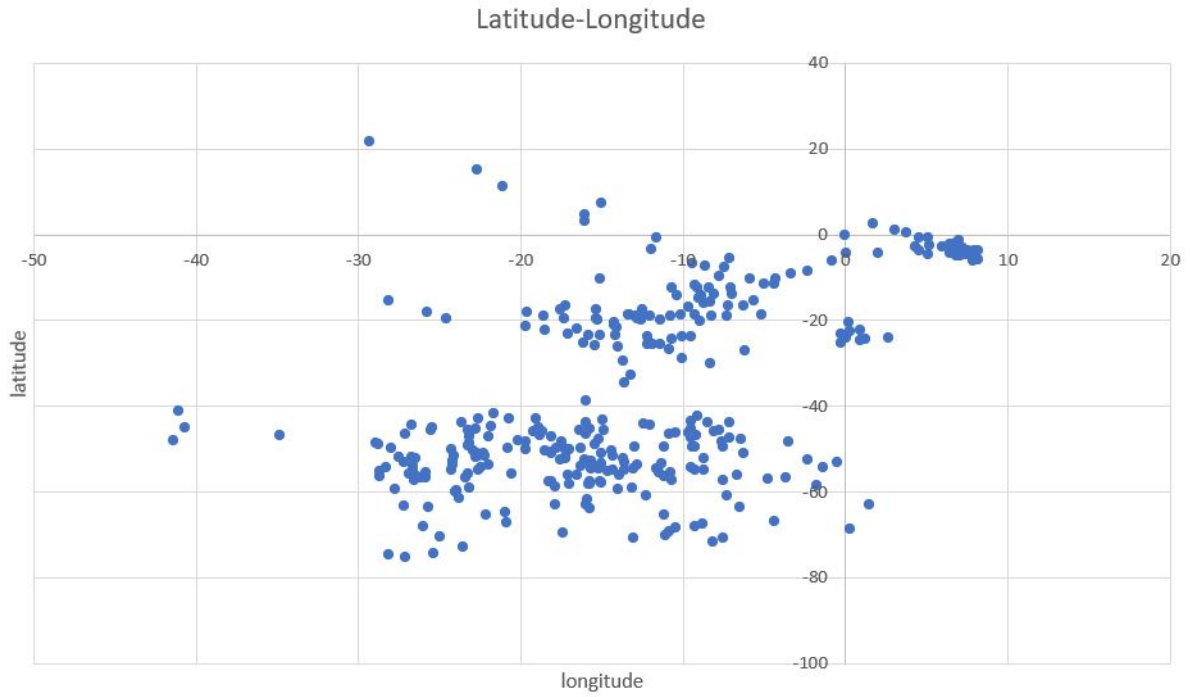
57

Figure 5.16: Diagram showing the movement of the probe without considering the altitude, like in a plane parallel to the Earth surface

5.2.2 Velocity fluctuations

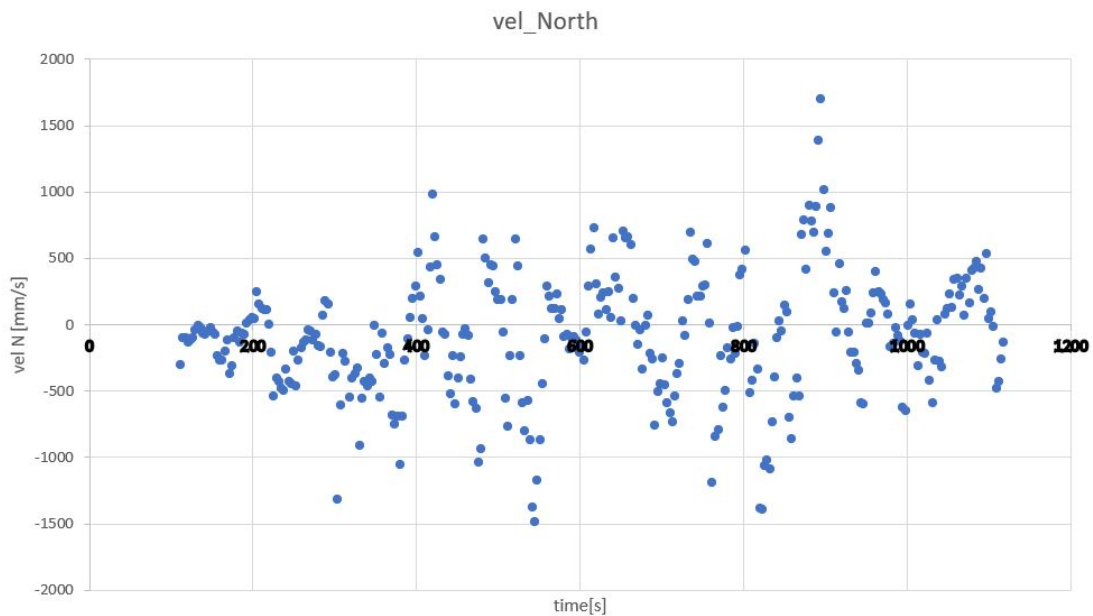Figure 5.17: Diagram showing the velocity in North direction, as the time varies. The negative speed values indicate that at that instant the radiosonde had a relative velocity with respect to the ground going South, the positive ones going North

58

Figure 5.18: Diagram showing the velocity in East direction, as the time varies. The negative speed values indicate that at that instant the radiosonde had a relative velocity with respect to the ground going West, the positive ones going East
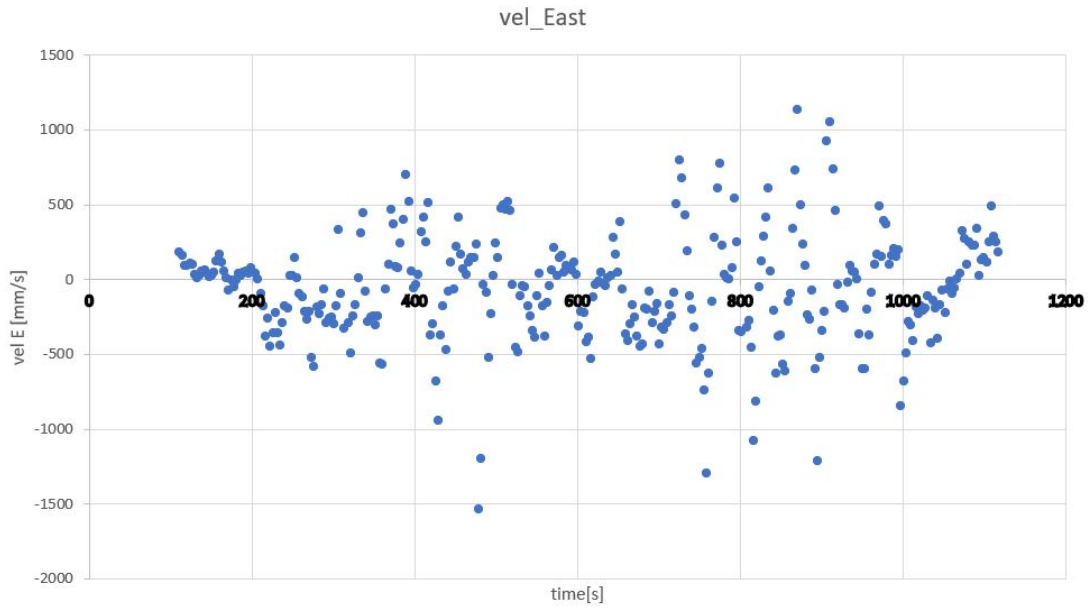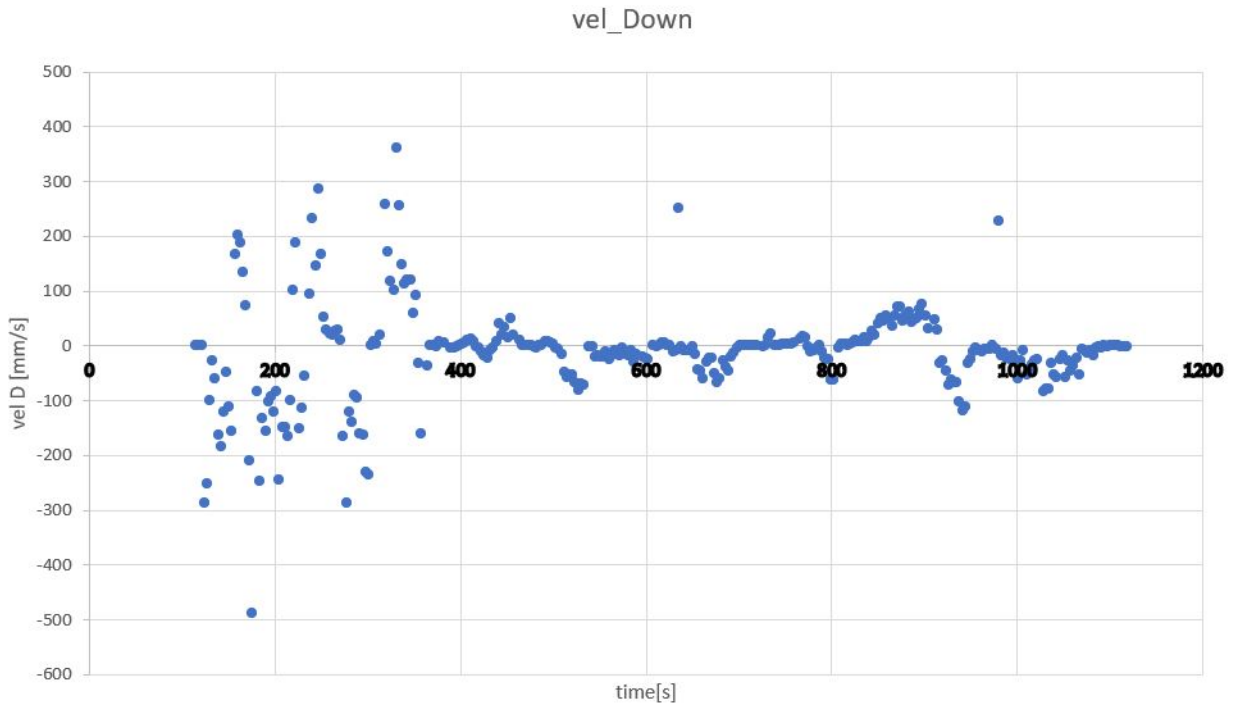

Figure 5.19: Diagram showing the velocity in down direction, as the time varies. The negative speed values indicate that at that instant the radiosonde had a relative velocity with respect to the ground going upward, the positive ones going downward

59

5.2.3 Atmospheric values measurement

Pressure

Figure 5.20: Pressure variation as a function of time during radiosonde flight

Figure 5.21: Pressure measurements at the respective altitudes

60

Temperature

Figure 5.22: Temperature variation as a function of time during radiosonde flight
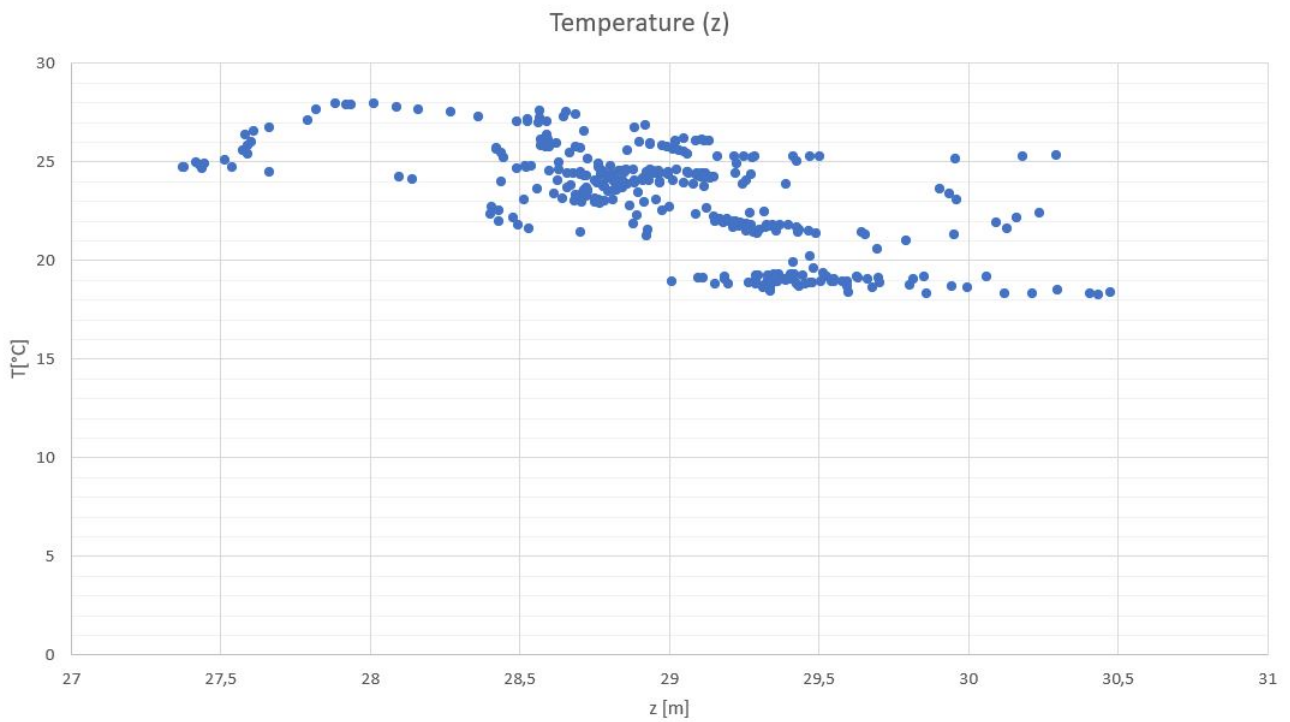
Figure 5.23: Temperature measurements at the respective altitudes

61
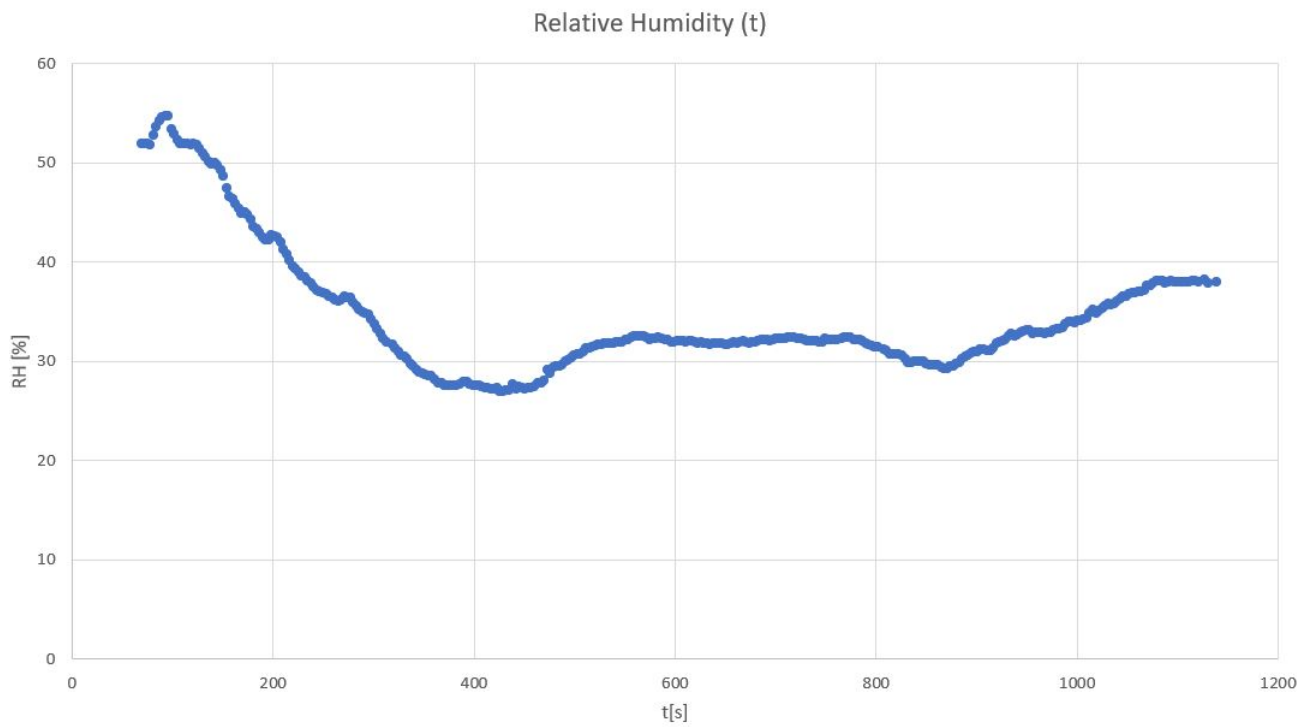
Relative humidity

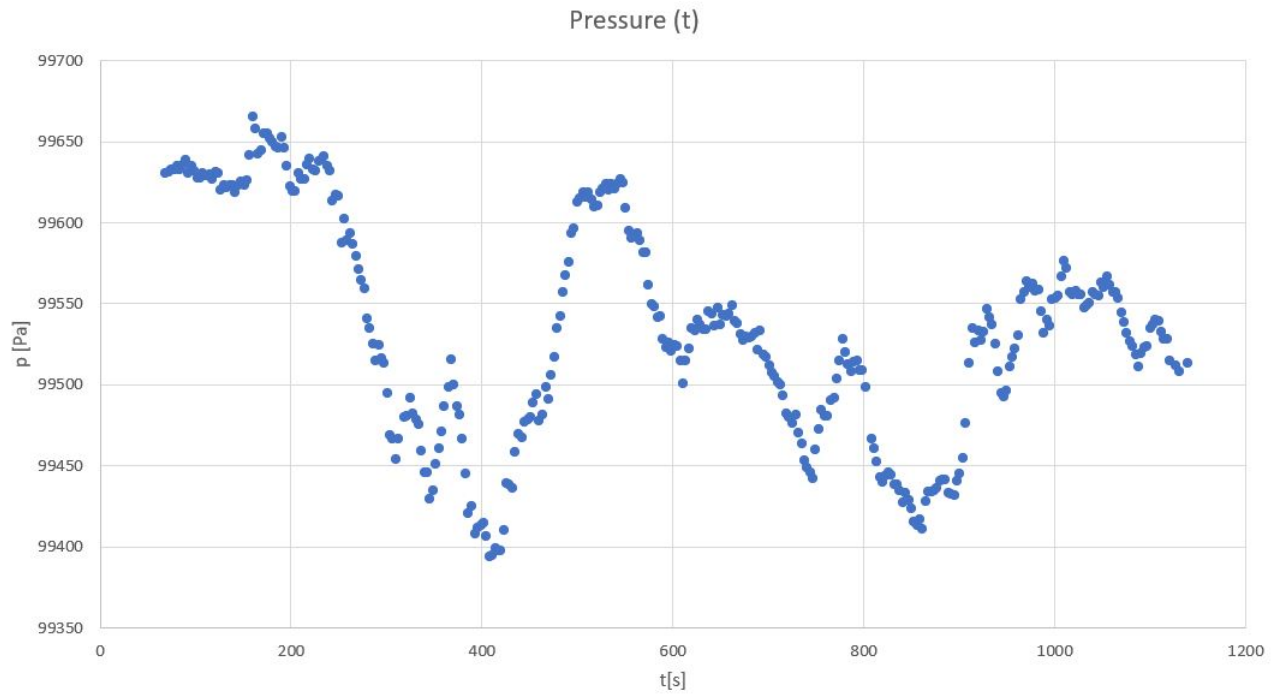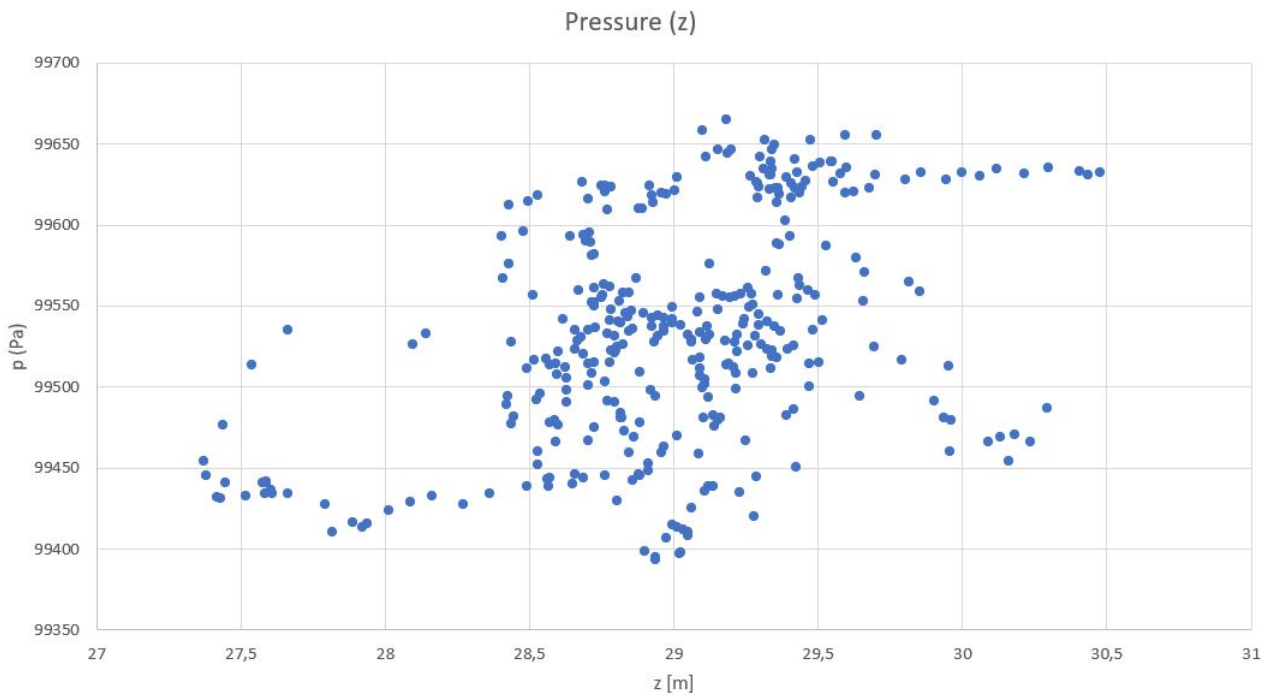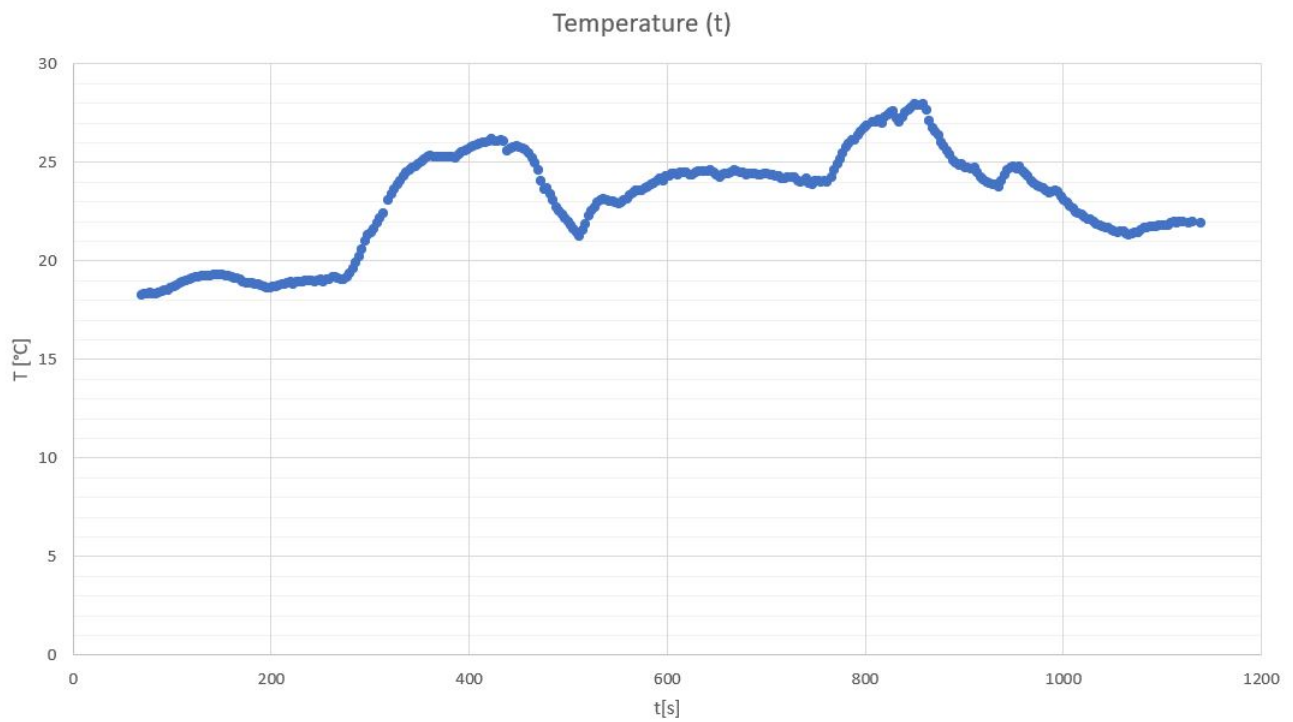Figure 5.24: Relative humidity variation as a function of time during radiosonde flight
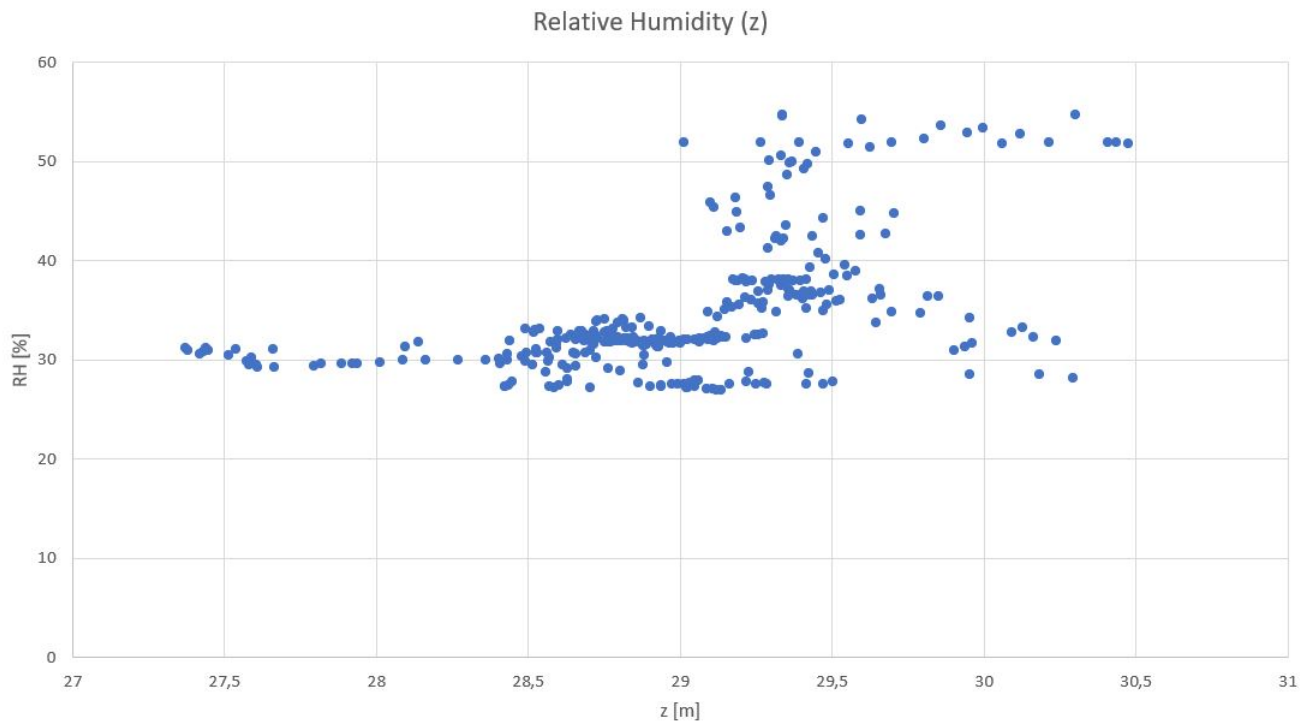
Figure 5.25: Relative humidity measurements at the respective altitudes

5.2.4 Tests on the resistance of the material and the coating to humidity absorption

Finally, a static test was carried out to assess the material's ability to withstand high humidity conditions, even for long periods of time, without deteriorating or becoming significantly heavy. Mater-Bi balloons were thus realized with the two coatings that in [3] gave the best results:

- 2 balloons coated with Carnauba Wax + SiO_2 nanoparticles

- 2 balloons coated with Carnauba Wax + Pine Resin

The samples were weighed, inflated and tied on the terrace of the PoliTo for 1 day. The environmental conditions (pressure, temperature, humidity, wind gusts) in which they were left was monitored thanks to specific sensors represented in Figures **??** throughout the experiment.

Figure 5.26: The sensors used to assess the climatic conditions

63

Figure 5.27: One of the four balloons inflated with helium

The sensors reported the relative humidity trend, with an average in 24 hours of 78%, with a value over 90% for about 5 hours. The average temperature was about 10^oC.

At the end of the 24 hours, the balloons were completely deflated and weighed again. In the table in Figures 5.28 the weights before and after the experiment are represented. Since the balloons have not undergone a weight variation of more than a tenth of a gram

id	ballon material	coating	diameter (cm)	old weight (g)	new weight (g)
A1	materBi	carnauba wax + pine resin	12,7	1,4	1,4
A2	materBi	carnauba wax + pine resin	12	1	1
B1	materBi	carnauba wax + SiO2 (silicon nanoparticles)	14	1,3	1,3
B2	materBi	carnauba wax + SiO2 (silicon nanoparticles)	12,7	1,3	1,3

Figure 5.28: Data related to balloon involved in the experiment, before and after

in more than 24 hours, it is reasonable to assume that the material, especially thanks to the use of coatings, will resist the atmospheric agents well and will not compromise future experiments, which however will not last much more than an hour.

Chapter 6

Conclusions

This thesis work initially illustrated the issues concerning the incomplete knowledge that science has at present regarding several steps about the evolution of clouds, the growth of droplets and the consequent development of rain. It has been illustrated how turbulence within the clouds considerably complicates the understanding of the phenomena taking place inside the clouds, but it is also demonstrated how turbulent phenomena considerably modify various phases of the development of droplets.

It was subsequently explained how the lack of information is partly due to a scarcity of data from in-situ measurament, especially from Lagrangian measurements, that are passive tracking of trajectory fluctuations.

It was also illustrated the Horizon2020 Innovative Training Network Cloud-Micro-Physics-Turbulence-Telemetry (MSCA-ITN-COMPLETE) project, which aims to develop a small radiosonde capable of floating in the clouds and transmitting Lagrangian-type information in real time. It has been explained the operating principle of the probe, the procedures for selecting the material with which the balloon is made, as well as the role of all radio-probe components.

Subsequently, the production protocol for the balloon developed in the IIT Smart Materials laboratory was established: the dimensions and shape that the balloon must have for the various altitudes at which it will fly, the weight of the individual components, the various procedures for placing the sensors inside, to build a balloon which is both resistant and capable of faithfully following the trajectories of the current.

Finally, the various tests carried out until now on the various components of the radio-probe have been reported. The very first tests in which the various sensors were tested showed excellent results, apart from the drone test, in which vibrations from the UAV disturbed the sensors' reading. Then a test was carried out in which the sensors were placed in an aerostatic balloon capable of travelling thousands of km and reaching the highest layers of the atmosphere, with highly acceptable results: the transmission system continued to send valid data up to 14 km and for over 30 minutes. A complete test was also carried out in which the Mater-Bi balloon was also subjected to a satisfactory response, both from the material of the balloon and the production method developed in IIT, as well as from the quality of the oscillations reported by the sensors inside it. Finally, an experiment in which the coating material's resistance to high humidity conditions was to be tested without getting damaged and heavy, showed excellent results, confirming the choice made in previous works [3].

The radio-probe as a whole still shows many points where it needs to be enhanced in the future. However, from the analyses and tests described in this thesis, it can be observed that the work done until now, although in a fully preliminary phase, can result useful to understand how a floating probe of the size of ours is able to track passively the fluctuations of the current. The probe has also proved to be capable of transmitting information correctly and reliably, with adequate temporal and spatial intervals.

Ringraziamenti

Colgo innanzitutto l'occasione per manifestare profonda gratitudine alla professoressa Daniela Tordella, relatrice di questa tesi, senza la quale non avrei potuto concludere il mio percorso universitario con questo splendido progetto. Un altro importante ringraziamento va ai dottori Athanassia Athanassiou e Giovanni Perotto, il quale in IIT mi ha accolto e guidato nel migliore dei modi, sempre gentile e disponibile ad aiutarmi. Grazie ancora a Myriam Paredes e Shahbozbek Abdunabiev per essere stati delle figure di riferimento sempre pronte ad aiutarmi in questo progetto.

Grazie alla mia famiglia per il supporto morale ed economico che non è mai mancato in questi anni: grazie a mia mamma per i suoi consigli e le sue carezze, anche e soprattutto per quelle a distanza; grazie a mio papà per essere sempre stato una guida pratica, efficiente ed amorevole in tutti i momenti; grazie a Luigi perchè quando si ha un fratello così dalla propria parte, diventa tutto più semplice. Grazie ancora a mia nonna, mio nonno, zio Lele, zia Rosa, Delia, Gio e anche Minù.

Un grazie immenso all'Alle, la mia forza, la mia felicità, il mio mondo, a lei devo la sicurezza con cui affronto le sfide: qualunque cosa accada, lei è in grado di farmi sentire fortunato con una naturalezza sconvolgente.

Grazie ancora a Giulia, Andrea e Filippo, che mi hanno accolto dal primo momento e mi hanno sempre fatto sentire a casa quando questa mi era lontana. Grazie anche a Zorro e la Tripa.

Infine, un enorme grazie va a tutti gli amici (ormai abbondantemente sparsi per il mondo) che hanno condiviso con me la spensieratezza di questi anni: quelli eterni di Palmi; quelli di Torino che mi hanno visto raggiungere questo traguardo; quelli che mi hanno "adottato" e fatto divertire a Modena; infine anche quelli con cui cui ho condiviso l'ultima esperienza di Genova.

Whole bibliography

[1] T. Basso, M. Iovieno, S. Bertoldo, G. Perotto, F. Canavero, G. Perona, A. Athanassiou, and D. Tordella, "Disposable radiosondes for tracking lagrangian fluctuations inside warm clouds", *2017 IEEE-APS Topical Conference on Antennas and Propagation in Wireless Communications (APWC)*, pp. 189–192, 2017.

[2] "Horizon 2020; Call: H2020-MSCA-ITN-2015-ETN - Proposal Submission Forms", *Research Executive Agency*, vol. 675675, 2015.

[3] T. Basso, G. Perotto, C. Musacchio, A. Merlone, A. Athanassiou, and D. Tordella, "Evaluation of Mater Bi Polyactic Acid as materials for biodegradable innovative mini-radiosondes to track small scale fluctuations within clouds", *Materials Chemistry and Physics*, vol. 253, p. 123 411, 2020.

[4] A. M. Society. (). Glossary of Meteorology (June 2000): Relative Humidity, [Online]. Available: `https://web.archive.org/web/20110707113357/http://amsglossary.allenpress.com/glossary/search?p=1&query=relative+humidity&submit=Search`. 2011-07-07.

[5] ——, (). Glossary of Meteorology (June 2000): Cloud, [Online]. Available: `https://web.archive.org/web/20081220034950/http://amsglossary.allenpress.com/glossary/search?id=cloud1`. 2008-12-20.

[6] U. S. Navy. (). Naval Meteorology and Oceanography Command (2007). Atmospheric Moisture, [Online]. Available: `https://web.archive.org/web/20090114165909/http://www.navmetoccom.navy.mil/pao/Educate/WeatherTalk2/indexatmosp.htm`. January 14, 2009.

[7] W. M. Organization. (). International Cloud Atlas, [Online]. Available: `https://cloudatlas.wmo.int/en/clouds-definitions.html`.

[8] H. Pruppacher and J. Klett, *Microphysics of Clouds and Precipitation*. Springer Science+Business Media B.V., 2010, ISBN: 978-0-7923-4211-3.

[9] Beard and Ochs, "Warm Rain Initiation: An Overview of Microphysical Mechanisms", *Journal of Applied Meteorology*, vol. 32, pp. 608–625, 1993.

[10] W. Grabowski and L. Wang, "Growth of cloud droplets in a turbulent environment", *Annual Reviews*, vol. 45, pp. 293–324, 2013.

[11] P. Prabhakaran, S. Weiss, A. Krekhov, A. Pumir, and E. Bodenschatz, "Can hail and rain nucleate cloud droplets?", *APS*, vol. 119, p. 128 701, 2017.

[12] P. Jonas, "Turbulence and cloud Microphysics", *Atmospheric Research*, vol. 40, pp. 283–306, 1996.

[13] V. Khvorostyanov and J. Curry, "Toward the theory of stochastic condensation in clouds. Part I: A general kinetic equation", *J. Atmos. Sci.*, vol. 56, pp. 3985–3996, 1999.

[14] B. Devenish, P. Bartello, J. Brenguier, L. Collins, W. Grabowski, R. IJzermans, S. Malinowski, M. Reeks, J. Vassilicos, L. Wang, and Z. Warhaft, "Droplet growth in warm turbulent clouds", *Q. J. R. Meteorol. Soc.*, vol. 138, pp. 1401–1429, 2012.

[15] L. Thomas, W. Wojciech, W. Grabowski, and B. Kumar, "Diffusional growth of cloud droplets in homogeneous isotropic turbulence: DNS, scaled-up DNS, and stochastic model", *Atmospheric Chemistry and Physics*, vol. 159, pp. 1–21, 2020.

[16] M. Pinsky and A. .Khain, "Fine structure of cloud droplet concentration as seen from the Fast-FSSP measurements. Part I: Method of analysis and preliminary results", *J. Appl. Met.*, vol. 40, pp. 1515–1537, 2001.

[17] J. Brenguier and L. Chaumat, "Droplet spectra broadening in cumulus clouds. Part I: Broadening in adiabatic", *J. Atmos. Sci*, vol. 58, pp. 628–641, 2001.

[18] J. Warner, "The Microstructure of Cumulus Cloud. Part I. General Features of the Droplet Spectrum", *J. Atmos. Sci*, vol. 26, pp. 1049–1059, 1969.

[19] J.Brenguier, "Observations of cloud microstructure at the centimeter scale", *J. Appl. Meteorol.*, vol. 32, pp. 783–793, 1993.

[20] E. Bodenschatz, S. Malinowski, R. Shaw, and F. Stratmann, "Can we understand clouds without turbulence?", *American Association for the Advancement of Science*, vol. 327, pp. 970–971, 2010.

[21] H.Siebert, S.Gerashenko, A.Gylfason, K.Lehmann, L.R.Collins, R.A.Shaw, and Z.Warhaft, "Towards understanding the role of turbulence on droplets in clouds: In situ laboratory measurements", *Atmospheric Research*, vol. 97, pp. 426–437, 2010.

[22] H.Siebert, K.Lehmann, and M.Wendisch, "Observations of Small-Scale Turbulence and Energy Dissipation Rates in the Cloudy Boundary Layer", *J. Atmos. Sci.*, vol. 63, pp. 1451–1466, 2006.

[23] A.Seifert, L. Nuijens, and B. Stevens, "Turbulence effects on warm-rain autoconversion in precipitating shallow convection", *Q. J. R. Meteorol. Soc.*, vol. 136, pp. 1753–1762, 2010.

[24] Y. Xue, L. Wang, and W. Grabowski, "Growth of cloud droplets by turbulent collision–coalescence", *J. Atmos. Sci.*, vol. 65, pp. 331–356, 2008.

[25] C. Franklin, "A warm rain microphysics parameterization that includes the effect of turbulence", *J. Atmos. Sci.*, vol. 65, pp. 1795–1816, 2008.

[26] R.A.Shaw, W.C.Reade, Collins, and Verlinde, "Preferential concentration of cloud droplets by turbulence: effects on the early evolution of cumulus cloud droplet spectra", *J. Atmos. Sci*, vol. 55, pp. 1965–1976, 1998.

[27] O.Ayala, B.Rosa, Wang, and W.W.Grabowski, "Effects of turbulence on the geometric collision rate of sedimenting droplets", *New J. Phys.*, vol. 10, 2008.

[28] P. Vaillancourt, M. Yau, P. Bartello, and W. Grabowski, "Microscopic approach to cloud droplet growth by condensation. Part II: Turbulence, clustering, and condensational growth", *J. Atmos. Sci*, vol. 59, pp. 3421–3435, 2002.

[29] S. Chen, P. Bartello, M. Yau, P. Vaillancourt, and K. Zwijsen, "Cloud Droplet Collisions in Turbulent Environment: Collision Statistics and Parameterization", *J. Atmos. Sci*, vol. 73, pp. 621–636, 2016.

[30] E. Woittiez, H. Jonker, and L.M.Portela, "On the combined effects of turbulence and gravity on droplet collisions in clouds: a numerical study", *J. Atmos. Sci.*, vol. 66, pp. 1926–1943, 2009.

[31] Y. Zhou, A. Wexler, and L. Wang, "Modelling turbulent collision of bidisperse inertial particles", *J. Fluid Mech*, vol. 433, pp. 77–104, 2001.

[32] T. Yang and S. Shy, "Two-way interaction between solid particles and homogeneous air turbulence: particle settling rate and turbulence modification measurements", *J. Fluid Mech*, vol. 526, pp. 171–216, 2005.

[33] R. Monchaux, M. Bourgoin, and A. Cartellier, "Preferential concentration of heavy particles: a Voronoi analysis", *Phys. Fluids*, vol. 22, p. 103 304, 2010.

[34] M.R.Maxey and J.J.Riley, "Equation of motion for a small rigid sphere in a non-uniform flow", *Phys. Fluids*, vol. 26, p. 883, 1983.

[35] W. C. de Rooy, P. Bechtold, K. Fröhlich, C.Hohenegger, H.Jonker, D. Mironov, A. P. Siebesma, J. Teixeira, and J. Yano, "Entrainment and detrainment in cumulus convection: an overview", *Royal Metereological Society*, vol. 139, pp. 1–19, 2012.

[36] P. Dimotakis, "Turbulent mixing", *Annu. Rev. Fluid Mech.*, vol. 37, pp. 329–356, 2005.

[37] J. Westerweel, C. Fukushima, J. M. Pedersen, and J. Hunt, "Momentum and scalar transport at the turbulent/non-turbulent interface of a jet", *J. Fluid Mech.*, vol. 631, pp. 199–230, 2009.

[38] C. Lu, S.Niu, Y.Liu, and A. Vogelmann, "Empirical relationship between entrainment rate and microphysics in cumulus clouds", *American Geophysical Union*, vol. 40, pp. 2333–2338, 2013.

[39] F.Burnet and J. Brenguier, "Observational study of the entrainment-mixing process in warm convective clouds", *J. Atmos. Sci.*, vol. 64, pp. 1995–2011, 2007.

[40] J. Brenguier and W. Grabowski, "Cumulus entrainment and cloud droplet spectra: a numerical model within a two-dimensional dynamical framework", *J. Atmos. Sci.*, vol. 50, pp. 120–136, 1993.

[41] S. Lasher-Trapp, W.A.Cooper, and A. Blyth, "Broadening of droplet size distributions from entrainment and mixing in a cumulus cloud", *Q. J. R. Meteorol. Soc.*, vol. 131, pp. 195–220, 2005.

[42] S. Businger, R. Johnson, and R. Talbot, "Scientific Insights from Four Generations of Lagrangian Smart Ballon", *Atmospheric Research*, vol. 87, pp. 1539–1554, 2006.

[43] M.Paredes, S. Bertoldo, C. Lucianaz, and M. Allegretti, "Ultra-light disposable radio probes for atmospheric monitoring", *EGU General Assembly Conference Abstracts*, vol. 20, p. 1389, 2018.

[44] CLOUD-MyPhyTuTel, "Ideas concerning ultra-light radiosondes", 2014.

[45] A. Wixted, P. Kinnaird, H. Larijani, A. Tait, A. Ahmadinia, and N. Strachan, "Evaluation of LoRa and LoRawan for wireless sensor networks", *2016 IEEE SENSORS*, pp. 1–3, 2016.

[46] O. Rorato, S. Bertoldo, C. Lucianaz, M. Allegretti, and R. Notarpietro, "An Ad-Hoc Low Cost Wireless Sensor Network for Smart Gas Metering", *Wireless Sensor Network*, vol. 5(3), pp. 61–66, 2013.

[47] M. Paredes, "COMPLETE Workshop: Data and model integration in fluid mechanics", *Imperial College London*, December 17 - 19 2019.

[48] J. D. Bois, R. Multhauf, and C. Ziegler, "The invention and development of the radiosonde: Smithsonian studies in history and technology", *Smithsonian Institution Press (Washington, DC)*, 2002.